University of Stavanger

Faculty of Science and Technology

MASTER'S THESIS

Study program/ Specialization: Petroleum Engineering, Reservoir Engineering	Spring semester, 2011 Open access
Writer: Ørjan Tveteraas	…… (Writer's signature)
Faculty supervisor: Aksel Hiorth External supervisor(s): -	
Title of thesis: A Study of Pressure Decay in a Closed CO_2-water System	
Credits (ECTS): 30	
Key words: Pressure decay, diffusion, diffusivity, advection, CO2, carbon dioxide, water, analytical.	Pages: 60 + front page + enclosure: 7 Stavanger, June 15, 2011

A Study of Pressure Decay in a Closed CO_2-water System

Ørjan Tveteraas

Thesis for the Degree of Master of Science
Department of Petroleum Engineering
University of Stavanger
June 15, 2011

University of Stavanger

Abstract

Analytical and semi-analytical solutions to the diffusion equation have been obtained in an effort to model pressure decay in a closed CO_2-water system. Various boundary conditions that include different physical effects and simplifications have been investigated. Experimental data have been interpreted qualitatively and quantitatively by making use of the analytical solutions. Numerical modelling of the system in question has also been explored. It has been concluded that the pressure decay can not exclusively be described by a diffusion process, and that advection currents increase the rate of mass transfer between the gas and liquid phase. It has been found that advection becomes less dominant compared to diffusion in late times of the pressure decay experiment. The experimental data has been interpreted in terms of a time-dependent effective diffusion coefficient that initially is two orders of magnitude greater than the diffusivity of CO_2 in water, and that gradually decreases towards the literature value. The diffusion-only model that has been put forward is found to accurately predict pressure decay in CO_2-bitumen, and methane-pentane systems.

Acknowledgements

I would like to extend my sincere and utmost gratitude to my supervisor, Aksel Hiorth, who has provided me with guidance and support throughout the process of writing this thesis. I also wish to thank Janne Pedersen for her help with the lattice Boltzman modelling.

Ørjan Tveteraas
Stavanger, June 15, 2011

Contents

1 Introduction

Carbon Dioxide (CO_2) is a gas that has been subject to much debate. While being blamed for causing global warming, it is also vital to life on earth, as well as having many industrial uses. Because of the problem of global warming, geological storage of CO_2 has been considered. When CO_2 is injected for storage it will come in contact with water and dissolve into it. Understanding and quantifying the processes that lead to dissolution of CO_2 into water is therefore important. Another area where knowledge about the dissolution of CO_2 in water is of interest, is when CO_2 is injected into petroleum reservoirs to increase recovery. In this process the CO_2 may come in contact with water, either when it comes in contact with previously injected water in the reservoir or aquifers surrounding the reservoir, as well as when the gas is injected together with water in a so called WAG[1] or SWAG[2] injection.

A method to experimentally determine diffusion coefficients of gases in liquids was introduced by Riazi in 1996 [1]. This method has been called the pressure decay method. When a gas is in contact with a liquid in a closed system, such as in a PVT cell, the pressure will decrease in the cell due to the fact that the gas dissolves in the liquid, thus taking up less volume. The method is based on the fact that the time it takes to reach equilibrium, the point where the liquid is saturated with the gas, is determined by the diffusion processes acting in the system. Originally applied to petroleum fluids, the pressure decay method has been successful in determining diffusion coefficients in many oil-gas systems. The method has been attractive because of its convenience, simplicity and accuracy [2].

Although pressure decay experiments on CO_2-water systems have not been as extensively used as for petroleum systems, some studies can be found in the literature. Farajzadeh et al. [3] have carried out pressure decay experiments involving CO_2 and water, and has put forward a theoretical interpretation of the observed effects. Pressure decay experiments have also been carried out by Time et al. [4] at the University of Stavanger in order to study the dissolution of CO_2 in water.

In order to understand the results from a pressure decay experiment, both quantitatively and qualitatively, it is useful to have a mathematical model that describes the system in question. The main focus of this thesis has been to find an analytical model that can adequately describe pressure decay in a closed CO_2-water system. Several approaches with different boundary conditions and assumptions have been used to this end. Experimental results have been interpreted based on comparison with the analytical model. Numerical simulations using the lattice Boltzmann method have also been implemented in an attempt to shed further light on the processes at work.

The impact of advection has been of particular interest. A solution containing CO_2 will be denser than pure water. This leads to instabilities that cause

[1] Water-Alternating-Gas. A method to increase oil production where water and gas is alternately injected into the reservoir for periods of time.

[2] Simultaneous-Water-and-Gas. Water and gas is injected simultaneously into the reservoir in an effort to increase oil production.

advection currents. The effect advection has on the rate of pressure decay during different stages of the experiment has been investigated .

2 Theory

2.1 Solubility of CO_2

The following reactions govern the solubility of CO_2(g) in distilled water [5]:

$$\begin{array}{lcll} CO_2(g) & & \rightleftharpoons & CO_2(aq)\ , \\ CO_2(aq) + H_2O & & \rightleftharpoons & H_2CO_3, \\ H_2CO_3 & & \rightleftharpoons & HCO_3^- + H^+, \\ HCO_3^- & & \rightleftharpoons & CO_3^{2-} + H^+, \\ OH^- + H^+ & & \rightleftharpoons & H_2O. \end{array}$$

When the pH is low (pH < 8) the generation of CO_3^{2-}can be neglected. The last reaction describes the autoprotolysis of water. Combining the first three reactions gives:

$$CO_2(g) + H_2O \rightleftharpoons HCO_3^- + H^+.$$

According to the law of mass action [6] the equilibrium constant for this reaction can be written as

$$K_{CO_2(g)} = \frac{a_{HCO_3^-} \cdot a_{H^+}}{a_{CO_2(g)}}. \tag{2.1}$$

where a is the activity[3] of each species. In order to simplify, it can be assumed that the activity equals the concentration m of the species in the solution. This is a valid assumption because of the low ionic strength of the CO_2-water solutions studied in this work. In the case of CO_2(g) the activity is equal to the partial pressure, $a_{CO_2(g)} = p_{CO_2(g)}$. In addition to the equilibrium constants, we also know that the system will be charge neutral,

$$m_{H^+} = m_{HCO_3^-} + m_{OH^-}.$$

At equilibrium we thus have

$$\begin{aligned} m_{H^+} &= \frac{K_{CO_2(g)} p_{CO_2(g)}}{m_{H^+}} + \frac{1}{K_{OH^-} \cdot m_{H^+}} \\ \Rightarrow m_{H^+} &= \sqrt{K_{CO_2(g)} p_{CO_2(g)} + \frac{1}{K_{OH^-}}}. \end{aligned}$$

$K_{OH^-} = 10^{14.05}$ at 25°C, so $\frac{1}{K_{OH^-}}$ can be neglected. From equation (2.1) we then get an expression for the concentration of HCO_3^- in solution.

$$m_{HCO_3^-} = \sqrt{K_{CO_2(g)} p_{CO_2(g)}}.$$

[3] The activity is a measure of the effective concentration of a species, and is treated as a dimensionless quantity.

From the definition of $K_{H_2CO_3}$, and the above expressions for m_{H^+} and $m_{HCO_3^-}$, it follows that

$$m_{HCO_3^-} = \frac{K_{CO_2(g)} p_{CO_2(g)}}{K_{H_2CO_3}}.$$

The conventional definition of the equilibrium constant K implies that $\frac{\text{mol}}{\text{l}}$ is used as the unit for concentration, and that atm is used as the unit for partial pressure. The total concentration of CO_2 in aqueous form is then

$$m_{\text{total}} = m_{H_2CO_3} + m_{HCO_3^-} \approx \frac{K_{CO_2(g)}}{K_{H_2CO_3}} p_{CO_2(g)}, \tag{2.2}$$

where the concentration of HCO_3^- is so small compared to the concentration HCO_3 that it has been neglected.

For the purposes of these calculations H_2CO_3 and $CO_2(aq)$ have been treated as the same species. In reality, the concentration of $CO_2(aq)$ dominates over the concentration of H_2CO_3 in a ratio of 386 to 1 (at ambient conditions) [5]. Equation (2.2) is analogous to Henry's law, $P = HC$, where P is the partial pressure of CO_2 in the gas phase , and C is the concentration of dissolved CO_2. When SI units are to be used, the Henry's law constant is defined as follows:

$$H \left[\frac{\text{m}^3\text{Pa}}{\text{mol}}\right] = 101.3 \frac{K_{H_2CO_3}}{K_{CO_2(g)}}.$$

The Henry's law constant, as it is calculated here, will give the sum of the concentrations of $CO_2(aq)$ and H_2CO_3 at equilibrium.

2.2 Transport mechanisms

2.2.1 Diffusion

Diffusion describes the process where random movement of particles causes matter to be transported from regions of higher to lower concentration. The transfer of mass is proportional to the concentration gradient. In 1855, Adolf Fick derived the laws of diffusion. Fick's first law of diffusion is an expression for the diffusive flux [7]:

$$\overrightarrow{J} = -D\nabla C, \tag{2.3}$$

where $\overrightarrow{J}$ is a vector describing the flux of particles in each direction $\left(\frac{\text{mol}}{\text{m}^2\text{s}}\right)$, and D is the diffusion coefficient. Fick's second law of diffusion, also known as the *diffusion equation* predicts how the concentration distribution changes with time:

$$D\nabla^2 C = \frac{\partial C}{\partial t}. \tag{2.4}$$

The diffusion equation can be derived from the continuity equation and Fick's first law. A finite region will have the following amount of particles:

$$\int_V C\,dV.$$

The flux of particles out of the region is:

$$\int_S \overrightarrow{J}\cdot\overrightarrow{n}\,dS,$$

where $\overrightarrow{n}$ is a normal unit vector pointing out of the domain enclosed by S. The source/sink term is given by:

$$\int_V A^*\,dV,$$

where A^* is rate of concentration change. Mass conservation can thus be written

$$\frac{d}{dt}\int_V C\,dV = -\int_S \overrightarrow{J}\cdot\overrightarrow{n}\,dS + \int_V A\,dV.$$

Use of the divergence theorem, and the Du Bois-Reymond lemma gives:

$$\begin{aligned}
&\frac{d}{dt}\int_V C\,dV = -\int_V \nabla J\,dV + \int_V A\,dV \\
\Rightarrow\quad & \frac{\partial C}{\partial t} + \nabla J = A \\
\Rightarrow\quad & \frac{\partial C}{\partial t} + \nabla(-D\nabla C) = A \\
\Rightarrow\quad & D\nabla^2 C + A = \frac{\partial C}{\partial t}.
\end{aligned} \tag{2.5}$$

Equation (2.5) is the general form of the diffusion equation. It is worth mentioning that, mathematically, diffusion of heat and diffusion of particles is treated identically. For a thorough derivation of the above equations, the reader is referred to [8].

2.2.2 Interface mass transfer

When a species (CO_2 in this work) is transported from a gaseous phase to a liquid phase, there are three mass transfer resistances that have to be overcome: the resistance in the gas phase, the resistance at the interface film, and the resistance in the liquid. Transport through the gas and liquid layers are driven by a concentration gradient. At the interface film, the transport processes are driven by a jump in concentration (concentrations are usually discontinuous at the interface between two materials [9]). The flux through the gas, J_{G}, and through the liquid, J_{L}, can be written as follows:

$$J_G = k_{\mathrm{G}}(P_{\mathrm{G}} - P_{\mathrm{interface}}),$$

$$J_{\mathrm{L}} = k_{\mathrm{L}}(C_{\mathrm{interface}} - C_{\mathrm{L}}),$$

where k_{G} and k_{L} are the interface transfer coefficients. The two expressions above should be equal, assuming no accumulation at the interface. See Figure 1 for a typical concentration distribution close to an interface. In the literature, the resistance at the interface film is often neglected, and only the resistances across the gas and liquid layers are used in the calculation of the interface transport coefficient. In some cases the resistance at the interface film should not be excluded [10]. When the resistance at the interface film is ignored, the concentration in the top layer of the liquid will be in instantaneous equilibrium with the overlying gas. When the film resistance is included, the concentration in the top layer of the liquid will gradually build up towards the equilibrium value. The flux into the liquid can be described as [11, 12]:

$$J = \frac{dn}{dt}\frac{1}{A} = k(C_{\mathrm{eq}} - C_L),$$

where n is number of moles, k is the interface film transfer coefficient, and C_{eq} is the liquid concentration in equilibrium with the overlying gas.

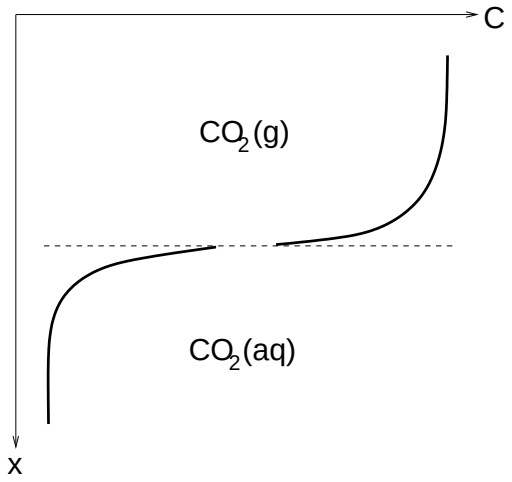

Figure 1: Concentration of CO_2 near the gas-liquid interface. The concentration in the liquid phase is determined from Henry's law, and will be lower than in the gas phase.

2.2.3 Advection

Advection[4] is an important mass transfer mechanism in which mass is transported by fluid motion. Advection currents often arise where there are density gradients that are negative in the direction of gravity, that is to say that the density increases upwards in the fluid. This is an arrangement that is potentially unstable. Because the force of gravity is stronger on the denser fluid, it may be 'pulled' down, while the less dense fluid flows upward. A common example of

[4]Historically, the terms *advection* and *convection* have been used interchangeably. However, according to Incropera et al. [9], it has become customary to use the term *advection* when referring to macroscopic fluid motion , and to the term *convection* when referring to the cumulative transport of molecular diffusion *and* macroscopic fluid motion. This definition has been used throughout this work.

this is when a fluid is heated from below. Heat causes the fluid to expand and become less dense, and advection may develop. Another case where advection currents can play a part is when a fluid absorbs another substance through an interface, such as when CO_2 is absorbed through the surface of water. The water containing CO_2 will be denser than pure water, and the resulting mixture becomes top-heavy, i.e. the fluid density increases upwards and the system becomes unstable. The force driven by the density gradient must overcome the viscous forces in the fluid in order for the instability to manifest itself. In other words, there is a critical density gradient necessary before flow starts to occur.

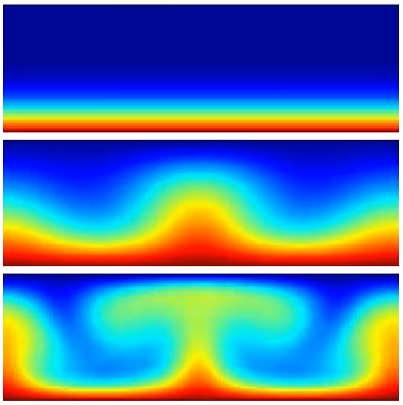

Figure 2: Illustration of advection occurring when fluid is heated from below. Image taken from lattice Boltzmann simulation of the Rayleigh-Bénard convection in Matlab. The Matlab code that runs the simulation depicted above can be found at http://www.lbmethod.org.

The challenge of determining the onset of the instability that occurs when a fluid is heated from below is called the Bénard problem [13]. The flow that occurs when the instability sets in is called Rayleigh-Bénard convection, and is one of the most commonly studied convection phenomena [14]. An analogy can be drawn between the Rayleigh-Bénard convection, and the convection that occurs when CO_2 dissolves into water from above. Considering that the diffusion of heat and the diffusion of molecules is treated the same way mathematically, and that the absorption of CO_2 from above causes an adverse density gradient much like when a fluid is heated from below, it is reasonable to conclude that the convection that occurs in the closed CO_2-water system studied in this work can be treated like the well studied Rayleigh-Bénard convection. More about Rayleigh-Bénard convection and how to determine the onset instability can be found in Appendix A.

2.3 The Laplace transform method

Several methods are used to solve partial differential equations, one of which is the Laplace transform method. The idea behind the method is to remove the time dependency, effectively converting the partial differential equation (PDE) into an ordinary differential equation (ODE). The inverse Laplace transform

is then applied to the solution of the ODE to obtain the final solution. The definition of the Laplace transform is:

$$\overline{F}(s) = \mathcal{L}\{F(t)\} = \int_0^\infty e^{-st} F(t) dt.$$

where $F(t)$ is the original function and $\overline{F}(s)$ is called the image function [15]. From this definition we have that

$$\mathcal{L}\left\{\frac{dF}{dt}\right\} = s\overline{F} - F(0).$$

Applying the Laplace transform to a PDE and its initial and boundary conditions, will in many cases lead to an easily solvable ODE. In order to find the inverse transform we have the following expression:

$$F(t) = \frac{1}{2\pi i} \int_{c+i\infty}^{c+i\infty} e^{ts} \overline{F}(s) ds,$$

where c is a complex number chosen by certain criteria. Obtaining the inverse transform can be a difficult and at times impossible process. Substantial efforts have been made to tabulate Laplace transforms as well as inverse Laplace transforms for a wide array of functions. If the inverse transform can not be found in tables or by conventional means, it is possible to calculate it numerically. Among such methods are the Gaver-Stehfest method [16], and a quotient difference method developed by de Hoog et al. [17]. These methods will find the value of the function in question for arbitrarily chosen values of t, while the analytical form of the function will remain unknown.

3 Analytical model

3.1 The physical system

The physical system to be modelled is a cell of constant volume containing a fixed amount of water with a gas cap of CO_2. The temperature is kept constant and there is no mass flux between the cell and its surroundings. As CO_2 dissolves into the water, $CO_2(g) \rightarrow CO_2(aq)$, the pressure in the cell decreases. The aim of the model is to accurately predict the pressure decay in the cell over time. Figure 3 provides an illustration of the physical system.

The exact mechanisms that determine the rate of pressure decline are unclear. For instance, experiments carried out by Time et al. [4] confirm the presence of advection currents in the cell during a pressure decay experiment. The impact of advection at different times of the experiment is unknown. It is also unclear whether there exists a significant interface film resistance to mass transfer. A number of scenarios will be investigated in this chapter in order to shed light on the processes at work.

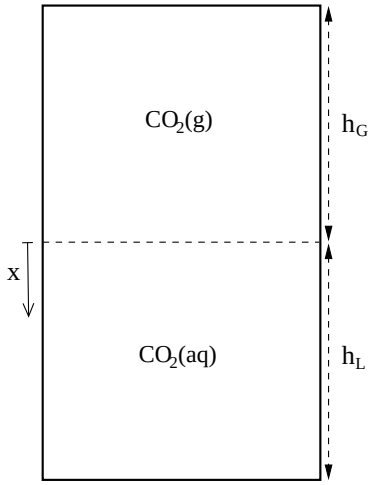

Figure 3: The CO_2-water system to be modelled.

3.2 Mathematical formulation

It is for the moment assumed that the transport mechanism is dominantly diffusion. The process can thus be described by the diffusion equation, see equation (2.4). The interface between water and CO_2 is assumed to be at instantaneous equilibrium according to Henry's law. In other words there is assumed to negligible interface film resistance between the two phases. The interface equilibrium concentration will decrease as the pressure decreases in the cell. Another simplifying assumption that is made is that the liquid volume remains constant, i.e. no swelling of the water due to the dissolution of CO_2. In order to keep calculations simple, the diffusion coefficient D, gas compressibility factor Z, and the Henry's law constant H, are assumed to be independent of pressure and concentration.

The physical system can be modelled in one dimension. The diffusion of CO_2 in the water can be described by equation (3.1).

$$D\frac{\partial C}{\partial x^2} = \frac{\partial C}{\partial t}, \quad 0 \leq x \leq h_{\mathrm{L}},\ t \geq 0. \tag{3.1}$$

It is assumed that the interface initially is at equilibrium with the overlying gas, while the concentration of CO_2 is zero everywhere else.

$$C = \begin{cases} \frac{P_{\mathrm{i}}}{H} & , z{=}0, t{=}0 \\ 0 & , z{>}0, t{=}0 \end{cases}. \tag{3.2}$$

According to the law of mass conservation, the flux of CO_2 into the liquid phase is equal to the flux of CO_2 out of the gas phase. The number of moles of CO_2 dissolved into the liquid phase (n_{d}) is therefore equal to the number of moles lost by the gas phase. Using the modified ideal gas law ($PV = ZnRT$) we get:

$$n_{\mathrm{d}} = \frac{V}{ZRT}\left[P_{\mathrm{i}} - P(t)\right] \Rightarrow \frac{dn_{\mathrm{d}}}{dt} = \frac{-V}{ZRT}\frac{dP}{dt}.$$

From Fick's first law we already have that: $\frac{dn_{\mathrm{d}}}{dt} = -DA\frac{\partial C}{\partial x}|_{x=0}$, which leads to:

$$\frac{\partial C}{\partial x}\Big|_{x=0} = \frac{V}{ZRTDA}\frac{dP}{dt} = \frac{h_{\mathrm{G}}}{ZRTD}\frac{dP}{dt}. \tag{3.3}$$

Henry's law allows us to express the pressure change as a concentration change at the interface:

$$P = HC \ \Rightarrow\ \frac{dP}{dt} = H\frac{\partial C}{\partial t}|_{x=0},$$

and we get the first boundary condition:

$$\frac{\partial C}{\partial x}\Big|_{x=0} = \alpha\frac{\partial C}{\partial t}\Big|_{x=0},\ t > 0. \tag{3.4}$$

where $\alpha = \frac{h_{\mathrm{G}}H}{ZRTD}$. The second boundary condition comes from the fact that there is no flux through the bottom of the container.

$$\frac{\partial C}{\partial x} = 0, \quad x = h_{\mathrm{L}}. \tag{3.5}$$

The diffusion boundary value problem presented above is solved by the method of Laplace transform. Both sides of equation (3.1) are transformed:

$$\begin{aligned} \mathcal{L}\left\{D\frac{\partial^2 C}{\partial x^2}\right\} &= \mathcal{L}\left\{\frac{\partial C}{\partial t}\right\} \\ \Rightarrow\ D\frac{d^2\overline{C}}{dx^2} &= \overline{C}s - C(x,0). \end{aligned}$$

For $x > 0$ we get the homogeneous ordinary differential equation :

$$\frac{d^2\overline{C}}{dx^2} - \frac{s}{D}\overline{C} = 0,$$

which has the general solution:

$$\overline{C}(x,s) = c_1 e^{\sqrt{\frac{s}{D}}x} + c_2 e^{-\sqrt{\frac{s}{D}}x}.$$

Laplace transform of the first boundary condition gives:

$$\frac{\partial \overline{C}}{\partial x}\Big|_{x=0} = \alpha \left(\overline{C}s - C(0,x)\right)|_{x=0}.$$

$C(0,0)$ is known from initial conditions.

$$\frac{\partial \overline{C}}{\partial x}\Big|_{x=0} = \alpha \left(\overline{C}s - \frac{P_{\mathrm{i}}}{H}\right)\Big|_{x=0} = \alpha \left((c_1+c_2)s - \frac{P_i}{H}\right). \tag{3.6}$$

The Laplace transform of the second boundary condition is:

$$\frac{\partial \overline{C}}{\partial x}\Big|_{x=h_{\mathrm{L}}} = c_1\sqrt{\frac{s}{D}}e^{\sqrt{\frac{s}{D}}h_{\mathrm{L}}} - c_2\sqrt{\frac{s}{D}}e^{-\sqrt{\frac{s}{D}}h_{\mathrm{L}}} = 0,$$

which yields:

$$c_1 = c_2 e^{-2\sqrt{\frac{s}{D}}h_{\mathrm{L}}}. \tag{3.7}$$

Differentiating the general form of the Laplace transformed solution:

$$\frac{\partial \overline{C}}{\partial x} = c_1\sqrt{\frac{s}{D}}e^{\sqrt{\frac{s}{D}}x} - c_2\sqrt{\frac{s}{D}}e^{-\sqrt{\frac{s}{D}}x} \tag{3.8}$$

$$\Rightarrow \frac{\partial \overline{C}}{\partial x}\Big|_{x=0} = c_1\sqrt{\frac{s}{D}} - c_2\sqrt{\frac{s}{D}}. \tag{3.9}$$

Inserting (3.6) in (3.9) while applying (3.7) gives:

$$\begin{aligned} c_1 &= \frac{P_{\mathrm{i}}e^{-2\sqrt{\frac{s}{D}}h_{\mathrm{L}}}}{H(s+\frac{1}{\alpha}\sqrt{\frac{s}{D}} + e^{-2\sqrt{\frac{s}{D}}h_{\mathrm{L}}}(s-\frac{1}{\alpha}\sqrt{\frac{s}{D}})}, \\ c_2 &= \frac{P_{\mathrm{i}}}{H(s+\frac{1}{\alpha}\sqrt{\frac{s}{D}} + e^{-2\sqrt{\frac{s}{D}}h_{\mathrm{L}}}(s-\frac{1}{\alpha}\sqrt{\frac{s}{D}})}, \end{aligned}$$

$$\Rightarrow \overline{C}(x,s) = \frac{P_{\mathrm{i}}(e^{\sqrt{\frac{s}{D}}x-2\sqrt{\frac{s}{D}}h_{\mathrm{L}}} + e^{-\sqrt{\frac{s}{D}}x})}{H(s+\frac{1}{\alpha}\sqrt{\frac{s}{D}} + e^{-2\sqrt{\frac{s}{D}}h_{\mathrm{L}}}(s-\frac{1}{\alpha}\sqrt{\frac{s}{D}})}. \tag{3.10}$$

This is the solution to the problem in Laplace space. In order to find the inverse Laplace transform, we simplify (3.10) by letting $h_{\mathrm{L}} \to \infty$.

$$\overline{C}(x,s) = \frac{P_{\mathrm{i}}}{H}\frac{e^{-\sqrt{\frac{s}{D}}x}}{\sqrt{s}(\sqrt{s}+\frac{1}{\alpha\sqrt{D}})}. \tag{3.11}$$

The inverse Laplace form of (3.11) can be found in [18]. The solution, which is valid in the infinite-acting period, is thus:

$$C(x,t) = \frac{P_\mathrm{i}}{H} \exp\left(\frac{x}{\alpha D} + \frac{t}{\alpha^2 D}\right) \operatorname{erfc}\left(\frac{x}{2\sqrt{Dt}} + \frac{\sqrt{t}}{\alpha\sqrt{D}}\right). \tag{3.12}$$

Using Henry's law and solving for $x = 0$ leads to an expression of pressure as a function of time:

$$P(t) = P_\mathrm{i} \exp\left(\frac{t}{\alpha^2 D}\right) \operatorname{erfc}\left(\frac{\sqrt{t}}{\alpha\sqrt{D}}\right). \tag{3.13}$$

This equation is identical to the expression put forward by Sheikha et al. [19] on the diffusivity of gases in bitumen. It is validated further by being consistent with the model developed by Etminan et al. [11], if interface film resistance is neglected and liquid height is infinite. The model presented here differs from the one used by Civan et al. [20], in that the equilibrium concentration is treated as constant by Civan et al.

For convenience in the analysis, the function for pressure decay can be expressed using dimensionless variables:

$$P_\mathrm{D} = \frac{P}{P_\mathrm{i}},$$

$$t_\mathrm{D} = \frac{t}{\alpha^2 D},$$

which leads to the following simple form of the expression for pressure decay:

$$P_\mathrm{D}(t_\mathrm{D}) = \exp(t_\mathrm{D}) \operatorname{erfc}\left(\sqrt{t_\mathrm{D}}\right).$$

Figure 4 shows how the dimensionless pressure decays as the dimensionless time increases.

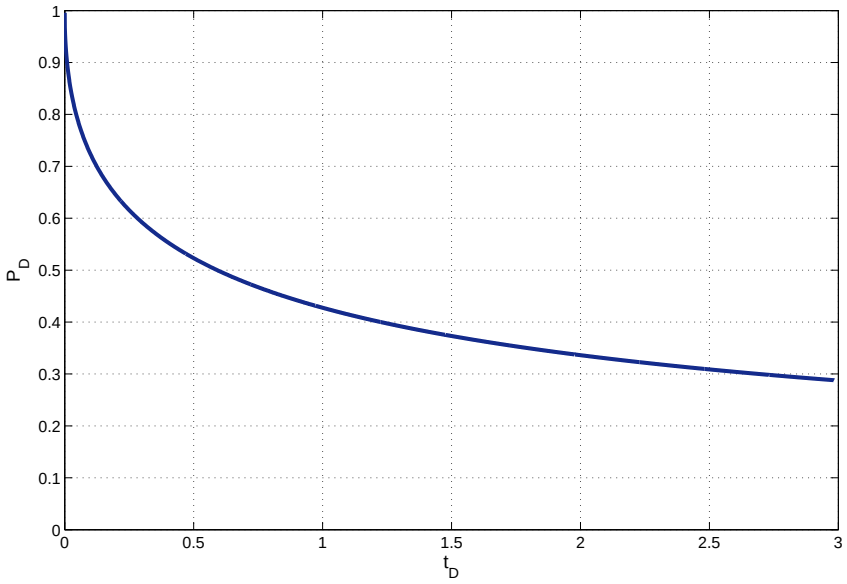

Figure 4: Predicted pressure decay in a closed CO_2-water system with infinite water column. Units on the axes are dimensionless.

3.3 Calculations with finite liquid height

At early times the the assumption of infinite liquid height will be valid. However, at a certain point the dissolved CO_2 will reach the bottom of the container, eventually leading to a significant decrease in the concentration gradient, slowing down the flux of CO_2 until it stops at the equilibrium concentration given by Henry's law. In order to investigate the effects of a finite water column, a semi-analytical approach is needed. The Laplace transform of Henry's law can be written

$$\overline{P}(s) = H\overline{C}(x,s)|_{x=0}.$$

Inserting the above equation into equation (3.10) evaluated at $x = 0$ provides an expression for the Laplace transformed pressure:

$$\overline{P}(s) = \frac{P_{\mathrm{i}}(e^{-2\sqrt{\frac{s}{D}}h_{\mathrm{L}}}+1)}{(s+\frac{1}{\alpha}\sqrt{\frac{s}{D}}+e^{-2\sqrt{\frac{s}{D}}h_{\mathrm{L}}}(s-\frac{1}{\alpha}\sqrt{\frac{s}{D}})}. \tag{3.14}$$

The inverse Laplace transform of the expression above can be obtained by numerical methods. An algorithm based on a method by de Hoog et al., which is commonly used in solving advection-diffusion problems [21], has been implemented in order to model the pressure decay over time. The algorithm can be found in [17]. Figure 5 shows the evolution of the gas pressure for different values of the liquid height.

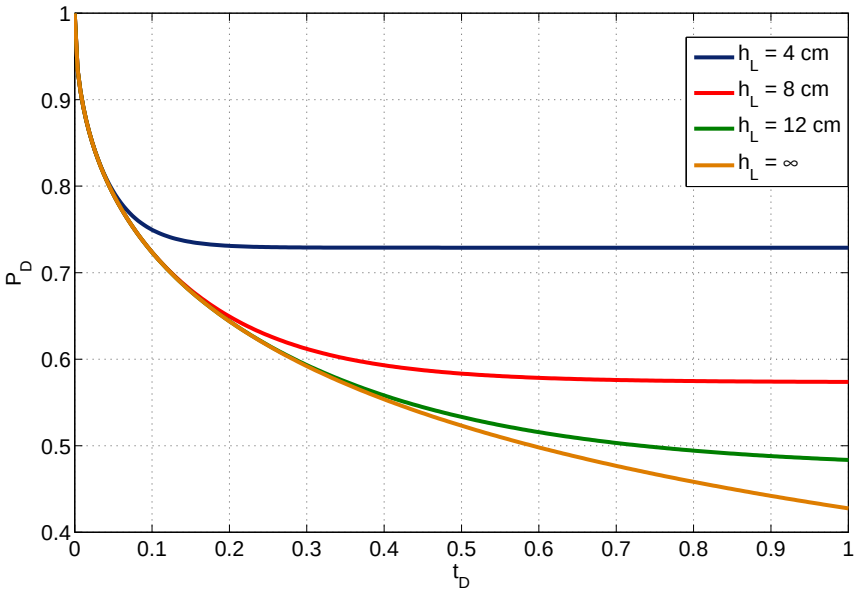

Figure 5: Pressure decay for cases with finite water column compared to the infinite-acting model. Dimensionless axes have been used. Besides the liquid height, the parameters used are the listed in Table 3. The plot is independent of the chosen diffusivity.

3.4 Initial concentration

3.4.1 Homogeneous distribution

In the previous sections there has been assumed to be no dissolved CO_2 initially. There are cases, however, when there will exist an initial concentration of CO_2 in the water. This scenario will for example be of interest when modelling a pure diffusion process at late times of a pressure decay experiment, after advection has ceased (as has been done in Section 5.2.3). A diffusion driven process, with an initial concentration distribution determined by the convection up to that point, would then continue the pressure decay. If this initial concentration is assumed to be homogeneous, we have the initial condition:

$$C = \begin{cases} C_\mathrm{i}, & t{=}0, z{>}0 \\ \frac{P_\mathrm{i}}{H}, & t{=}0, z{=}0 \end{cases}.$$

We define

$$C^* = C - C_\mathrm{i}. \tag{3.15}$$

The initial conditions will thus be

$$C^* = \begin{cases} \frac{P_\mathrm{i}}{H} - C_\mathrm{i}, & t{=}0, z{=}0 \\ 0, & t{=}0, z{>}0 \end{cases}.$$

The differential equation (3.1) is still valid,

$$D\frac{\partial^2 C^*}{\partial x^2} = \frac{\partial C^*}{\partial t}, \quad 0 \le x \le h_\mathrm{L},\, t \ge 0.$$

The boundary conditions will be the same as in the case of zero initial concentration. Solving the partial differential in the infinite-acting case gives:

$$\begin{aligned} C^*(z,t) &= \left(\frac{P_\mathrm{i}}{H} - C_\mathrm{i}\right) \exp\left(\frac{x}{\alpha D} + \frac{t}{\alpha^2 D}\right) \operatorname{erfc}\left(\frac{x}{2\sqrt{Dt}} + \frac{\sqrt{t}}{\alpha\sqrt{D}}\right) \\ \Rightarrow\ C(z,t) &= C + \left(\frac{P_\mathrm{i}}{H} - C_i\right) \exp\left(\frac{x}{\alpha D} + \frac{t}{\alpha^2 D}\right) \operatorname{erfc}\left(\frac{x}{2\sqrt{Dt}} + \frac{\sqrt{t}}{\alpha\sqrt{D}}\right), \end{aligned}$$

which leads to

$$P(t) = HC_\mathrm{i} + (P_\mathrm{i} - HC_\mathrm{i}) \exp\left(\frac{t}{\alpha^2 D}\right) \operatorname{erfc}\left(\frac{\sqrt{t}}{\alpha\sqrt{D}}\right). \tag{3.16}$$

When the height of the water column is finite, the solution can be found in Laplace space. The Laplace transform of (3.15) gives

$$\overline{C}^* = \overline{C} - \frac{C_\mathrm{i}}{s} \quad \Rightarrow \quad \overline{P}^* = \overline{P} - \frac{HC_\mathrm{i}}{s}$$

and we have

$$\overline{P}(s) = \frac{HC_\mathrm{i}}{s} + \frac{(P_\mathrm{i} - HC_\mathrm{i})(e^{-2\sqrt{\frac{s}{D}}h_\mathrm{L}} + 1)}{(s + \frac{1}{\alpha}\sqrt{\frac{s}{D}} + e^{-2\sqrt{\frac{s}{D}}h_\mathrm{L}}(s - \frac{1}{\alpha}\sqrt{\frac{s}{D}})}. \tag{3.17}$$

Figure 6 illustrates how the pressure decays for different homogeneous initial concentrations.

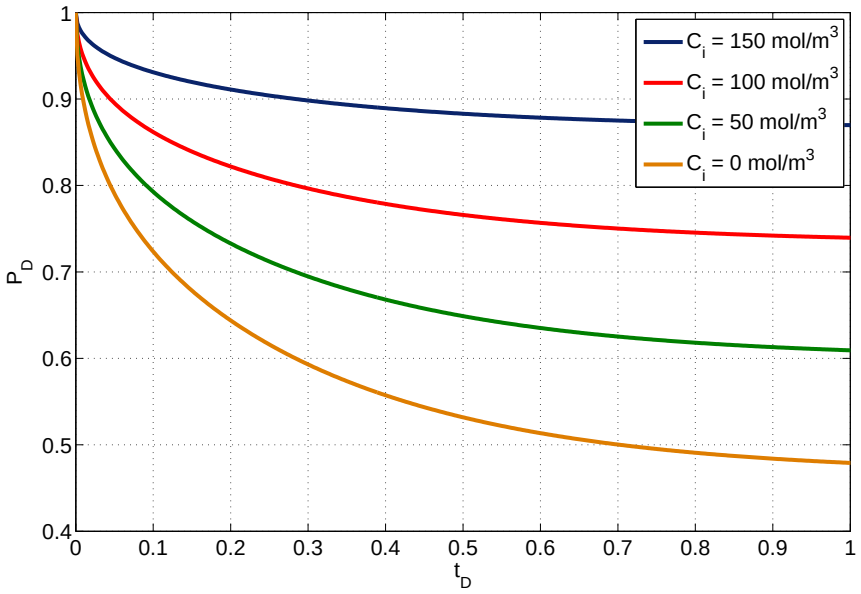

Figure 6: Pressure decay for finite liquid height and different initial concentrations. The initial concentrations in the solution is listed in the legend of the figure. The initial *equilibrium* concentration is set to 200 $\frac{mol}{m^3}$. Standard diffusion coefficient of CO_2 in water has been used and the liquid height is 0.1 m.

3.4.2 Heterogeneous distribution

Scenarios where the initial concentration distribution can not be assumed to be homogeneous may also be of interest. For instance, if early-time advection does not result in adequate mixing of the solution before diffusion starts to dominate, the concentration distribution may be heterogeneous. For mathematical simplicity it is here assumed that the initial distribution is linear,

$$C = \begin{cases} \frac{P_i}{H}, & t{=}0, x{=}0 \\ \kappa_1 x + \kappa_2, & t{=}0, x{>}0 \end{cases}.$$

The highest concentration possible will be the initial equilibrium concentration, and there should therefore be an upper limit to the maximum value of $\kappa_1 x + \kappa_2$ in order to keep the mathematical representation physically correct. If the concentration increases with depth, the expression below must be satisfied.

$$\kappa_1 h_{\mathrm{L}} + \kappa_2 \leq C_{\mathrm{eq}}.$$

The Laplace transformed diffusion equation is written

$$D\frac{d^2\overline{C}}{dx^2} = \overline{C}s - C(x,0) = \overline{C}s - (\kappa_1 x + \kappa_2). \tag{3.18}$$

Equation (3.18) is a non-homogeneous ordinary differential equation. As in Section 3.2, the homogeneous solution is

$$\overline{C}_{\mathrm{h}} = c_1 e^{\sqrt{\frac{s}{D}}x} + c_2 e^{-\sqrt{\frac{s}{D}}x}.$$

It can easily be shown that the particular solution is

$$\overline{C}_{\mathrm{p}} = \frac{\kappa_1 x + \kappa_2}{s}.$$

The general solution will then be

$$\overline{C}(x,s) = c_1 e^{\sqrt{\frac{s}{D}}x} + c_2 e^{-\sqrt{\frac{s}{D}}x} + \frac{\kappa_1 x + \kappa_2}{s}. \tag{3.19}$$

Differentiating the above expression and applying the boundary conditions gives the following:

$$\begin{aligned}
\left.\frac{\partial \overline{C}}{\partial x}\right|_{x=0} &= c_1\sqrt{\frac{s}{D}} - c_2\sqrt{\frac{s}{D}} + \frac{\kappa_1}{s} = \alpha\left(s(c_1 + c_2 + \frac{\kappa_2}{s}) - \frac{P_{\mathrm{i}}}{H}\right), \\
\left.\frac{\partial \overline{C}}{\partial x}\right|_{x=h_{\mathrm{L}}} &= c_1\sqrt{\frac{s}{D}}e^{\sqrt{\frac{s}{D}}h_{\mathrm{L}}} - c_2\sqrt{\frac{s}{D}}e^{-\sqrt{\frac{s}{D}}h_{\mathrm{L}}} + \frac{\kappa_1}{s} = 0.
\end{aligned}$$

The unknown constants, c_1 and c_2, can now be determined from the equations above.

$$\begin{aligned}
c_1 &= e^{-2\sqrt{\frac{s}{D}}h_{\mathrm{L}}} \cdot \frac{\frac{P_{\mathrm{i}}}{H} - \frac{\kappa_1}{\alpha s}\left[e^{-\sqrt{\frac{s}{D}}h_{\mathrm{L}}}(1-\alpha\sqrt{sD}) - 1\right] - \kappa_2}{s + \frac{1}{\alpha}\sqrt{\frac{s}{D}} + e^{-2\sqrt{\frac{s}{D}}h_{\mathrm{L}}}\left(s - \frac{1}{\alpha}\sqrt{\frac{s}{D}}\right)} - \frac{\kappa_1 e^{-\sqrt{\frac{s}{D}}h_{\mathrm{L}}}}{s\sqrt{\frac{s}{D}}}, \\
c_2 &= \frac{\frac{P_{\mathrm{i}}}{H} - \frac{\kappa_1}{\alpha s}\left[e^{-\sqrt{\frac{s}{D}}h_{\mathrm{L}}}(1-\alpha\sqrt{sD}) - 1\right] - \kappa_2}{s + \frac{1}{\alpha}\sqrt{\frac{s}{D}} + e^{-2\sqrt{\frac{s}{D}}h_{\mathrm{L}}}\left(s - \frac{1}{\alpha}\sqrt{\frac{s}{D}}\right)}.
\end{aligned}$$

Inserting c_1 and c_2 in equation (3.19) gives the expression for concentration in Laplace space:

$$\begin{aligned}
\overline{C}(x,s) = (e^{\sqrt{\frac{s}{D}}x - 2\sqrt{\frac{s}{D}}h_L} + e^{-\sqrt{\frac{s}{D}}x}) \cdot \frac{\frac{P_i}{H} - \frac{\kappa_1}{\alpha s}\left[e^{-\sqrt{\frac{s}{D}}h_L}(1-\alpha\sqrt{sD}) - 1\right] - \kappa_2}{s + \frac{1}{\alpha}\sqrt{\frac{s}{D}} + e^{-2\sqrt{\frac{s}{D}}h_L}\left(s - \frac{1}{\alpha}\sqrt{\frac{s}{D}}\right)} \\
+ \kappa_1\left(\frac{x}{s} - \frac{e^{\sqrt{\frac{s}{D}}x - \sqrt{\frac{s}{D}}h_L}}{s\sqrt{\frac{s}{D}}}\right) + \frac{\kappa_2}{s}.
\end{aligned} \tag{3.20}$$

Evaluating the above expression at $x = 0$, while applying Henry's law, yields the function for pressure decay:

$$\begin{aligned}
\overline{P}(s) = (e^{-2\sqrt{\frac{s}{D}}h_L} + 1) \cdot \frac{P_i - \frac{\kappa_1 H}{\alpha s}\left[e^{-\sqrt{\frac{s}{D}}h_L}(1-\alpha\sqrt{sD}) - 1\right] - \kappa_2 H}{s + \frac{1}{\alpha}\sqrt{\frac{s}{D}} + e^{-2\sqrt{\frac{s}{D}}h_L}\left(s - \frac{1}{\alpha}\sqrt{\frac{s}{D}}\right)} \\
- H\kappa_1\frac{e^{-\sqrt{\frac{s}{D}}h_L}}{s\sqrt{\frac{s}{D}}} + \frac{H\kappa_2}{s}.
\end{aligned} \tag{3.21}$$

The inverse Laplace transform of equation (3.21) has been done numerically, and the predicted pressure decay for different initial distributions can be seen in Figure 7.

In order to find a fully analytical solution for the infinite-acting case, an infinite liquid height is assumed ($h_{\mathrm{L}} \to \infty$). The expression for the pressure decay is reduced to

$$\overline{P}(s) = \frac{P_{\mathrm{i}} + \frac{\kappa_1 H}{\alpha s} - \kappa_2 H}{s + \frac{1}{\alpha}\sqrt{\frac{s}{D}}} + \frac{H\kappa_2}{s}.$$

In order to find the inverse Laplace transform of the above expression, it first has to be rewritten by the method of partial fractions. The inverse Laplace transform can then be found in [22]. Equation (3.22) is the resulting expression for pressure decay. Figure 8 shows a comparison between the infinite-acting model and the semi-analytical finite-acting model. Because of the assumption of infinite liquid height, the solution eventually becomes unphysical, and as time increases, the pressure goes towards infinity when $\kappa_1 > 0$.

$$\begin{aligned} P(t) &= (P_{\mathrm{i}} + \kappa_1 \alpha H D - \kappa_2 H) \exp\left(\frac{t}{\alpha^2 D}\right) \operatorname{erfc}\left(\frac{\sqrt{t}}{\alpha\sqrt{D}}\right) \\ &\quad + \kappa_1 H \sqrt{D}\left(2\sqrt{\frac{t}{\pi}} - \alpha\sqrt{D}\right) + \kappa_2 H. \end{aligned} \tag{3.22}$$

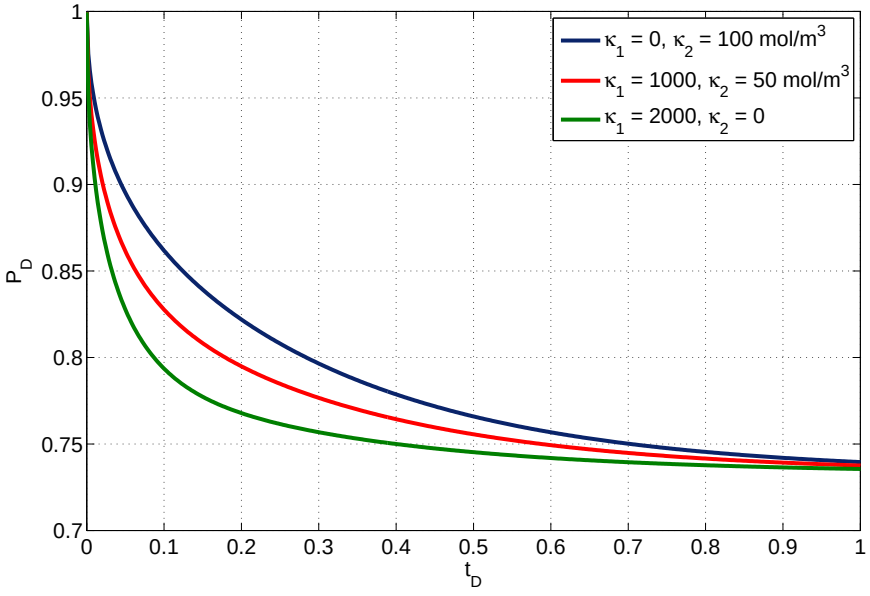

Figure 7: Predicted pressure decay with different initial distributions. Average initial concentration is in all cases equal to 100 $\frac{\mathrm{mol}}{\mathrm{m}^3}$. The initial equilibrium concentration is 200 $\frac{\mathrm{mol}}{\mathrm{m}^3}$. Surface concentration is specified (κ_2), and concentration increases linearly with depth. Standard diffusion coefficient of CO_2 in water has been used and the liquid height is 0.1 m.

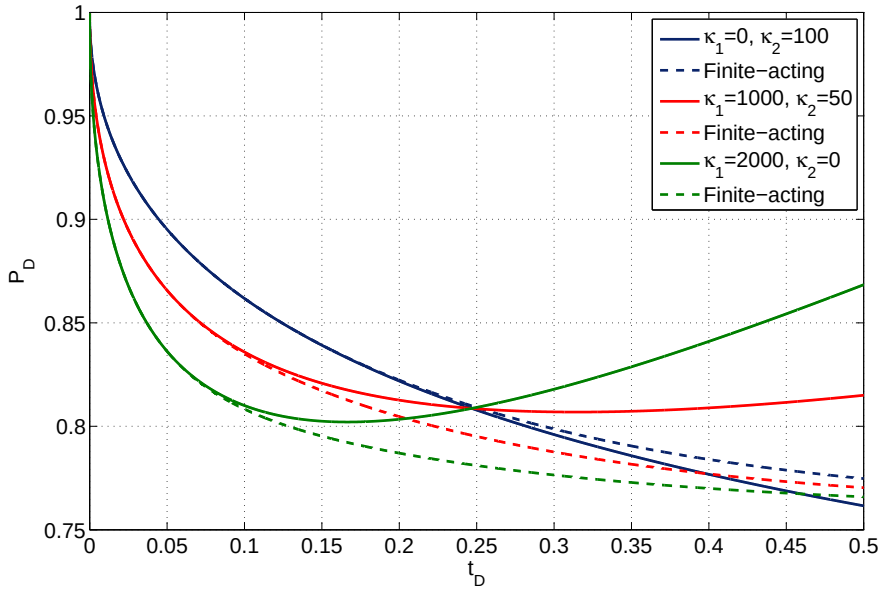

Figure 8: Predicted pressure decay for the infinite-acting model with linear initial distribution compared to the semi-analytical finite-acting model. Average initial concentration is in all cases equal to 100 $\frac{\text{mol}}{\text{m}^3}$. The initial equilibrium concentration is 200 $\frac{\text{mol}}{\text{m}^3}$.

3.5 Time-dependent diffusion coefficient

In many cases the diffusion coefficient can be considered to be constant. In reality it can potentially vary significantly in the time-frame of interest. Scenarios in which temperature or viscosity changes with time are examples of cases where diffusivity may be time-dependent. When transport phenomena in addition to diffusion are present, the system may be described by an *effective* diffusion coefficient that accounts for all significant transport processes. In the case of CO_2 dissolving in water, the effective diffusion coefficient may depend upon the amount of advection, and thus change over time. The following calculations are based on a time-dependent effective diffusion coefficient, $D = D(t)$. The diffusion equation becomes:

$$D(t)\frac{\partial^2 C}{\partial x^2} = \frac{\partial C}{\partial t}. \tag{3.23}$$

The diffusion equation with time-dependent diffusion coefficient is potentially very difficult to solve. According to Crank [7], the following substitution may in some cases be helpful:

$$dt = \frac{d\tau}{D(t)}.$$

Integration of the above equation leads to:

$$\tau(t) = \int_0^t D(t')dt'. \tag{3.24}$$

Equation (3.23) becomes:

$$\frac{\partial^2 C}{\partial x^2} = \frac{\partial C}{\partial \tau}.$$

The initial condition (3.2) is still valid, provided that $t = 0$ implies that $\tau = 0$. The first boundary condition (3.4) is a function of t, and becomes

$$\frac{\partial C}{\partial x}|_{x=0} = D(t)\alpha \frac{\partial C}{\partial \tau}|_{x=0} = \alpha_\tau \frac{\partial C}{\partial \tau}|_{x=0}$$

where $\alpha = \frac{h_G H}{D(t) \cdot ZRT}$ and $\alpha_\tau = \frac{h_G H}{ZRT}$. The second boundary condition remains the same. The Laplace transformed solution is

$$\overline{C}(x, s_\tau) = \frac{P_i(e^{\sqrt{s_\tau}x - 2\sqrt{s_\tau}h_L} + e^{-\sqrt{s_\tau}x})}{H(s_\tau + \frac{\sqrt{s_\tau}}{\alpha_\tau} + e^{-2\sqrt{s_\tau}h_L}(s_\tau - \frac{\sqrt{s_\tau}}{\alpha_\tau})}, \tag{3.25}$$

which leads to the following expression for the pressure decay in Laplace space:

$$\overline{P}(s_\tau) = \frac{P_i(e^{-2\sqrt{s_\tau}h_L} + 1)}{H(s_\tau + \frac{\sqrt{s_\tau}}{\alpha_\tau} + e^{-2\sqrt{s_\tau}h_L}(s_\tau - \frac{\sqrt{s_\tau}}{\alpha_\tau})} \tag{3.26}$$

The variable s has been given the subscript τ to emphasize that an inverse Laplace transform will yield a function of τ instead of t. If the solution is simplified to be infinite acting, it becomes:

$$\overline{C}(x, s_\tau) = \frac{P_i}{H} \frac{e^{-\sqrt{s_\tau}x}}{\sqrt{s_\tau}(\sqrt{s_\tau} + \frac{1}{\alpha_\tau})}.$$

Performing the inverse Laplace transform on the above expression gives:

$$C(x, \tau) = \frac{P_i}{H} \exp(\frac{x}{\alpha_\tau} + \frac{\theta}{\alpha_\tau^2})\text{erfc}(\frac{x}{2\sqrt{\tau}} + \frac{\sqrt{\tau}}{\alpha_\tau}), \tag{3.27}$$

and the expression for the expression decay as a function of the transformed time τ becomes:

$$P(\tau) = \frac{P_i}{H} \exp(\frac{\tau}{\alpha_\tau^2})\text{erfc}(\frac{\sqrt{\tau}}{\alpha_\tau}). \tag{3.28}$$

In order to find $P(t)$, the integral in equation (3.24) must be solved and inserted into the above expression. When an explicit expression for P is not available (when dealing with calculations concerning a finite water column), the procedure is similar: for every value of t, the corresponding value of τ is instead inserted into the algorithm that calculates P at that time.

3.6 Including interface film resistance

Up to this point instantaneous equilibrium has been assumed at the interface. Generally, there may exist an interface film resistance to mass transfer. For

instance, increased interface film resistance may arise from adsorption of surfactant molecules to the interface [3]. Such a scenario might arise in a CO_2-surfactant flooding that is performed to increase oil recovery. Also, the possibility that interface film resistance could be significant even in distilled water should not be ignored. The concentration at the aqueous side of the interface will gradually build up towards equilibrium concentration over time. In the notation used in this work, k is the interface film mass transfer coefficient, and $\frac{1}{k}$ is the resistivity factor. The situation where the interface is at instant equilibrium can be considered a special case, where $k \to \infty$. The flux from the gas to the interface is given by the expression below [11, 12].

$$J = k\left(C_{\text{eq}}(t) - C(x,t)|_{x=0}\right),$$

where C_{eq} is the equilibrium concentration of CO_2 given by Henry's law. Combining the above with Fick's first law (see Section 2.2.1) gives:

$$-D\frac{\partial C}{\partial x}\Big|_{x=0} = k\left(C_{\text{eq}}(t) - C(x,t)|_{x=0}\right). \tag{3.29}$$

Rearranging and differentiating with regards to t yields:

$$\frac{\partial C}{\partial t}\Big|_{x=0} - \frac{D}{k}\frac{\partial^2 C}{\partial x \partial t}\Big|_{x=0} = \frac{\partial C_{\text{eq}}}{\partial t}. \tag{3.30}$$

Equation (3.4) can in this case be written

$$\frac{\partial C_{\text{eq}}}{\partial t} = \frac{1}{\alpha}\frac{\partial C}{\partial x}\Big|_{x=0}. \tag{3.31}$$

From Equations (3.30) and (3.31) we thus have the boundary condition for gas-water interface:

$$\frac{\partial C}{\partial x}\Big|_{x=0} = \alpha\left[\frac{\partial C}{\partial t} - \frac{D}{k}\frac{\partial^2 C}{\partial x \partial t}\right]_{x=0}.$$

The Laplace transformed boundary condition is

$$\frac{\partial \overline{C}}{\partial x}\Big|_{x=0} = \alpha\left[s\overline{C} - C(x,0) - \frac{D}{k}(s\frac{\partial \overline{C}}{\partial x} - \frac{\partial C}{\partial x}|_{t=0})\right]_{x=0}.$$

Because the concentration is homogeneous initially, it follows that $\frac{\partial C}{\partial x}|_{t=0} = 0$. The boundary condition in Laplace space becomes

$$\frac{\partial \overline{C}}{\partial x}\Big|_{x=0} = \frac{\alpha}{(1+\frac{\alpha D}{k}s)}(s\overline{C} - \frac{P_{\text{i}}}{H})\Big|_{x=0}.$$

The expression for the concentration is found in the same manner as in Section (3.2).

$$\overline{C}(x,s) = \frac{P_i(e^{\sqrt{\frac{s}{D}}x - 2\sqrt{\frac{s}{D}}h_{\text{L}}} + e^{-\sqrt{\frac{s}{D}}x})}{H\left(s + \left(\frac{1}{\alpha} + \frac{Ds}{k}\right)\sqrt{\frac{s}{D}} + e^{-2\sqrt{\frac{s}{D}}h_{\text{L}}}\left[s - \left(\frac{1}{\alpha} + \frac{Ds}{k}\right)\sqrt{\frac{s}{D}}\right]\right)}. \tag{3.32}$$

In order to relate the aqueous concentration to the gas pressure, Henry's law, as well as the relationship between $C(x=0,t)$ and $C_{\text{eq}}(t)$, is used. Henry's law is in this case written

$$\overline{P}(s) = H\overline{C}_{eq}(s) \tag{3.33}$$

The Laplace transform of equation (3.29) yields

$$\overline{C}_{eq}(t) = \overline{C}(x,t)|_{x=0} - \frac{D}{k}\frac{\partial \overline{C}}{\partial x}\Big|_{x=0}. \tag{3.34}$$

Inserting (3.33) in (3.34) leads to

$$\overline{P}(s) = H\overline{C}(x,s)|_{x=0} - \frac{DH}{k}\frac{\partial \overline{C}}{\partial x}\Big|_{x=0}. \tag{3.35}$$

Equation (3.32) and its derivative is combined with the above equation to get equation (3.36), the expression for pressure in the Laplace domain. It is easy to see that the expression is reduced to equation (3.14), the case with no interface film resistance, when $k \to \infty$.

$$\overline{P}(s) = \frac{P_i\left[(e^{-2\sqrt{\frac{s}{D}}h_{\text{L}}}+1) - \frac{D}{k}\left(\sqrt{\frac{s}{D}}e^{-2\sqrt{\frac{s}{D}}h_{\text{L}}} - \sqrt{\frac{s}{D}}\right)\right]}{s + \left(\frac{1}{\alpha}+\frac{Ds}{k}\right)\sqrt{\frac{s}{D}} + e^{-2\sqrt{\frac{s}{D}}h_{\text{L}}}\left[s - \left(\frac{1}{\alpha}+\frac{Ds}{k}\right)\sqrt{\frac{s}{D}}\right]}. \tag{3.36}$$

The expression above has also been put forward by [11]. Numerical methods can be used to find the pressure as a function of time. Figure 9 illustrates how the pressure behavior changes when the interface film resistance is varied. It is the ratio D/k that governs the impact of the interface film resistance, i.e. higher diffusivity will make the interface film resistance more significant.

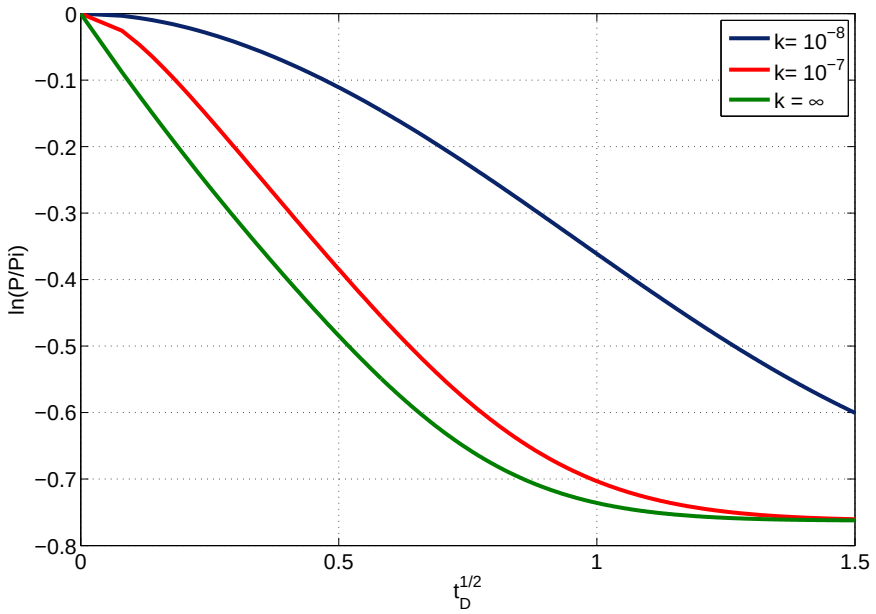

Figure 9: Predicted pressure decay for different interface film resistances. The diffusion coefficient is set to $D = 2 \cdot 10^{-9}\ \frac{\text{m}^2}{\text{s}}$.

3.7 Boundary condition at gas-liquid interface

3.7.1 Boundary conditions from published literature

There is no consensus on which boundary condition should be used at the gas-liquid interface. Researchers have been using boundary conditions ranging from simplified expressions that allow for analytical solutions to be obtained, to more complex expressions that include several physical effects. Which boundary condition is more appropriate depends on the fluids used and the conditions of the experiment [23]. Riazi [1], who first introduced the pressure decay method in 1996, considered both the equilibrium concentration and the position of the interface to vary with time. These variables were, however, treated as constants within certain time intervals, and the model was divided into discrete time steps. Later, Zhang et al. [24] modelled the problem using a constant Dirichlet[5] condition at the gas-liquid interface, while ignoring change of interface position due to swelling:

$$C(x,t)|_{x=0} = C_{\text{eq,final}}. \tag{3.37}$$

This makes analytical solutions easier to obtain than when alternative conditions are used. However, the assumption that the interface concentration is constant is not physically correct and may lead to errors when applying the model.

Upreti et al. [25] utilized a non-constant Dirichlet condition as the interface condition. Their study focused on a CO_2-bitumen system, and included the effect of swelling of the bitumen in their model. The boundary condition, which is more physically correct than the one used by Zhang et al., is as follows:

$$C(x,t) = C_{\text{eq,final}}(t).$$

In 2006, Sheikha et al. [26] introduced a new boundary condition that used the principle of mass conservation to equate the flux of mass leaving the gas phase to the flux into the liquid phase. The same relationship was used by Zhang et al. in order to relate mass flux to pressure decay, but simplifications lead to equation (3.37) being implemented in their model as their boundary condition. Sheikha et al. used the model in a study of dissolution of gases in bitumen. Farajzadeh et al. [3] also used this boundary condition when modelling the mass transfer of CO_2 into water. The boundary condition is written below, and is of the Neuman[6] type. The constant α is defined in Section 3.2.

$$\frac{\partial C}{\partial x}\Big|_{x=0} = \alpha \frac{\partial C}{\partial t}\Big|_{x=0}.$$

Civan et al. [12] applied a non-equilibrium boundary condition to the problem. It was assumed that there was an interface film resistance between the gas and liquid phase, and the interface concentration would consequently not be in equilibrium with the overlying gas. The theoretical equilibrium concentration

[5] The so called Dirichlet, or first-type, boundary condition specifies the values a solution has on the boundary of the domain.

[6] The Neuman, or second-type, boundary condition specifies the values the derivative of the solution has on the boundary of the domain.

was, as in the case of Zhang et al., considered constant and based on the final pressure. The expression for this Robin[7] boundary condition is:

$$-D\frac{\partial C}{\partial x}\Big|_{x=0} = k\left(C_{\text{eq,final}} - C(x,t)|_{x=0}\right).$$

In 2010, Etminan et al. [11] modified the boundary condition above to also include the time-dependency of the equilibrium concentration. The resulting model is more physically correct than the one developed by Civan et al., and it is more versatile then the one of Sheikha et al., as it allows for the existence of interface film resistance. The expression for this boundary condition is:

$$-D\frac{\partial C}{\partial x}\Big|_{x=0} = k\left(C_{\text{eq,final}}(t) - C(x,t)|_{x=0}\right).$$

3.7.2 Solution - constant Dirichlet BC

The constant boundary condition at the interface have been used as a simplification to the pressure decay problem because it makes analytical calculations easier. Modified pressure decay experiments have also been designed with this in mind, in which the pressure in the cell is kept constant, while pressure declines in an external tank supplying gas to the cell [2]. The mathematical problem is the same as in Section 3.2, except for the boundary condition at the interface. The Laplace transformed solution is thus:

$$\overline{C}(x,s) = c_1 e^{\sqrt{\frac{s}{D}}x} + c_2 e^{-\sqrt{\frac{s}{D}}x}.$$

The boundary condition at the gas-liquid interface is:

$$C(x,t)|_{x=0} = C_{\text{eq}}.$$

The constants A and B are determined from the boundary conditions:

$$c_1 = \frac{C_{\text{eq}}}{s(1+e^{2\sqrt{\frac{s}{D}}h_L})},$$

$$c_2 = \frac{C_{\text{eq}}}{s(1+e^{-2\sqrt{\frac{s}{D}}h_L})}.$$

The expression for the concentration in Laplace space thus becomes:

$$\overline{C}(x,s) = C_{\text{eq}}\left(\frac{e^{\sqrt{\frac{s}{D}}x}}{s(1+e^{2\sqrt{\frac{s}{D}}h_L})} + \frac{e^{-\sqrt{\frac{s}{D}}x}}{s(1+e^{-2\sqrt{\frac{s}{D}}h_L})}\right).$$

If we let the height of the water column go to infinity, the expression becomes:

$$C(x,s) = \frac{C_{\text{eq}}}{s}e^{-\sqrt{\frac{s}{D}}x}.$$

[7] The Robin, or third-type, boundary condition specifies a relationship between the values of the solution and its derivative on the boundary of the domain.

The inverse Laplace transform of the above expression (can be found in [18]) gives the infinite acting solution:

$$C(x,t) = C_{\text{eq}}\text{erfc}\left(\frac{x}{2\sqrt{Dt}}\right).$$

In order to calculate the pressure decay from the above equation, the gas law combined with the principle of mass conservation is used. The total number of moles dissolved into the water is:

$$n_{\text{d}}(t) = \int_0^\infty C(x,t)A\,dx = C_{\text{eq}}A\int_0^\infty \text{erfc}\left(\frac{x}{2\sqrt{Dt}}\right)dx$$

$$= \left[x\,\text{erfc}\left(\frac{x}{2\sqrt{Dt}}\right) - 2\sqrt{\frac{Dt}{\pi}}e^{\frac{-x^2}{4Dt}}\right]_0^\infty = 2C_{\text{eq}}A\sqrt{\frac{Dt}{\pi}}.$$

The expression for the pressure decay becomes

$$P(t) = \frac{ZRT\left[n_{\text{tot}} - n_{\text{d}}(t)\right]}{V} = P_{\text{i}} - \frac{2C_{\text{eq}}ZRT}{h_G}\sqrt{\frac{Dt}{\pi}}.$$

A significant discrepancy can be observed in the predicted pressure decay between the cases of constant and time-dependent surface concentration. The difference is apparent in Figure 10 when either the initial or the final equilibrium concentration is chosen as the surface concentration. However, the choice should depend upon whether early or late times of the experiment is to be studied.

The final equilibrium concentration is calculated as follows (see section 3.8 for calculation of final pressure):

$$C_{\text{eq}} = \frac{P_i h_G}{Hh_G + ZRTh_L}. \tag{3.38}$$

3.7.3 Solution - Robin BC with constant C_{eq}

A Robin boundary condition that accounts for interface film resistance is written below. Civan et al. [12] used this boundary condition and considered the equilibrium concentration to be constant.

$$J = -D\frac{\partial C}{\partial x}|_{x=0} = k\left(C_{\text{eq}} - C(x,t)|_{x=0}\right). \tag{3.39}$$

The mathematical formulation is otherwise the same as in section 3.2. The solution below is given by Crank [7], and is valid in the infinite acting period, i.e. $h_{\text{L}} \to \infty$.

$$\begin{aligned} C(x,t) &= C_{\text{eq}}\text{erfc}\left(\frac{x}{2\sqrt{Dt}}\right) \\ &\quad - C_{\text{eq}}\exp\left(\frac{kx}{D} + \frac{k^2t}{D}\right)\text{erfc}\left(\frac{x}{2\sqrt{Dt}} + k\sqrt{\frac{t}{D}}\right). \end{aligned} \tag{3.40}$$

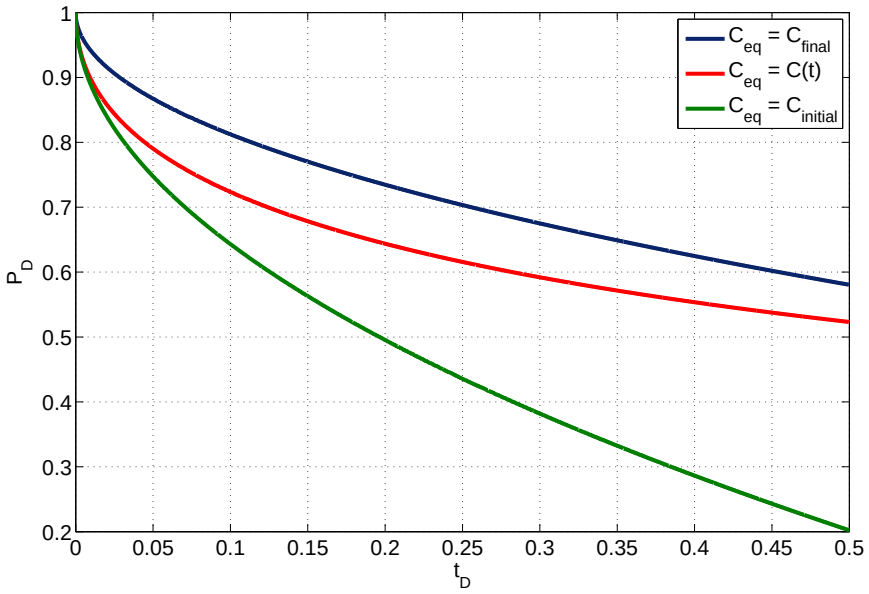

Figure 10: Predicted pressure decay for cases of constant surface concentration compared to when the concentration is time-dependent. Results are shown for surface concentrations at initial and final equilibrium. The liquid height is infinite, and the gas height is set to 0.1 m.

When the interface resistance goes to zero, $k \to \infty$, the solution becomes identical to the case with with the constant Dirichlet boundary from section 3.7.2. By integration of Equation (3.39) after inserting Equation (3.40) valued at at $x = 0$, it follows that the number of moles of the diffusing substance that has accumulated in the liquid is

$$n_{\mathrm{d}} = C_{\mathrm{eq}} A \frac{D}{k} \left[\exp\left(\frac{k^2 t}{D}\right) \operatorname{erfc}\left(k\sqrt{\frac{t}{D}}\right) - 1 + 2k\sqrt{\frac{t}{D\pi}} \right].$$

From the above equation and the gas law we get the expression for the pressure decay:

$$P(t) = P_{\mathrm{i}} - C_{\mathrm{eq}} \frac{ZRT}{h_G} \frac{D}{k} \left[\exp\left(\frac{k^2 t}{D}\right) \operatorname{erfc}\left(k\sqrt{\frac{t}{D}}\right) - 1 + 2k\sqrt{\frac{t}{D\pi}} \right].$$

From Figure 11 it can be observed that the discrepancy between the cases of constant and time-dependent equilibrium concentration is significant, but the difference is smaller for higher interfacial film resistances.

3.8 Validating the model

Calculating final pressure:

In order to validate the model, simple calculations can be performed to ensure that the late time values are correct. An expression for the equilibrium pressure

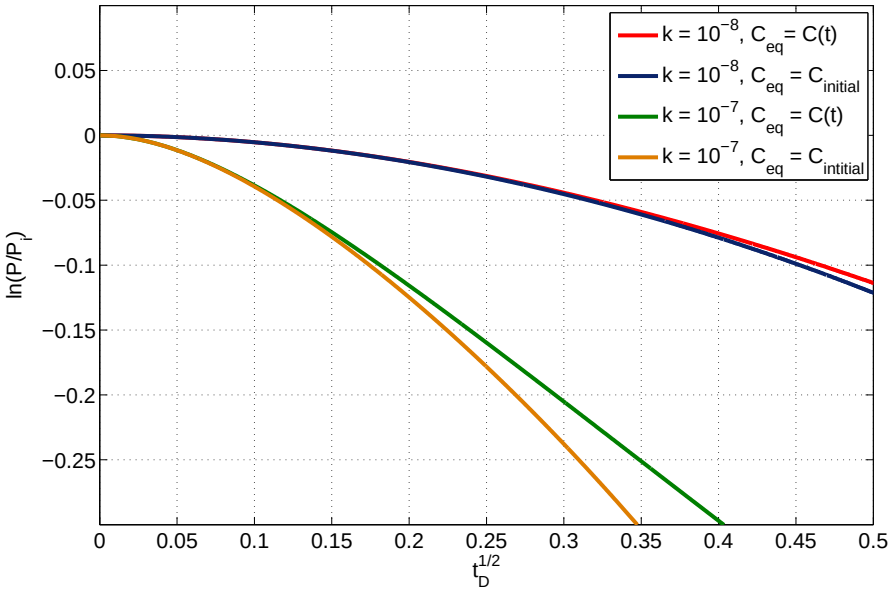

Figure 11: Predicted pressure decay when the Robin boundary condition with constant equilibrium concentration is used. Results are shown for surface concentration at initial equilibrium. Results for the model with time-dependent equilibrium concentration is also shown for comparison. The diffusivity $D = 2 \cdot 10^{-9}\ \frac{\mathrm{m}^2}{\mathrm{s}}$ has been used in the calculations. The liquid height is infinite, and the gas height is set to 0.1 m.

in a closed and finite CO_2-water system is derived using Henry's law, the gas law, and the law of mass conservation:

$$P_{\mathrm{D}}^{\mathrm{final}} = \frac{P^{\mathrm{final}}}{P_{\mathrm{i}}} = \frac{Hh_{\mathrm{G}}}{Hh_{\mathrm{G}} + ZRTh_{\mathrm{L}}}.$$

Numerical Laplace transform inversion:

The numerical inversion of Laplace transforms performed in this chapter have been carried out by the use of an algorithm based on a quotient difference method by de Hoog et al. A Matlab script for this method has been written by Hollenbeck [17]. In order to validate the results, calculations have also been carried out by the Gaver-Stehfest method for inverse Laplace transform. The Gaver-Stehfest algorithm can be found in [16]. Comparison of results based on the two methods can be seen in Figure 12. A near-perfect match can be observed.

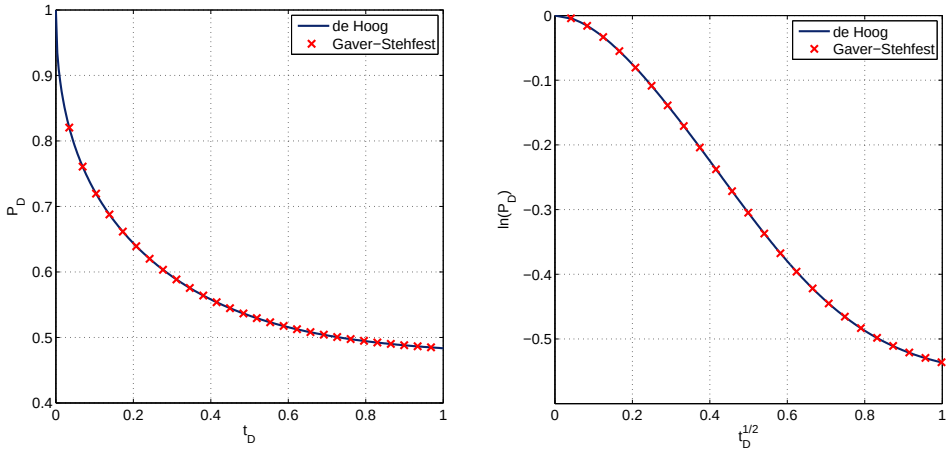

Figure 12: Comparison of semi-analytical results obtained by two different inverse Laplace transform algorithms. The left plot is for the finite-acting model from Section 3.3. The right plot is for the model with interface film resistance from Section 3.6.

4 Experimental results (hydrocarbon systems)

4.1 Pressure decay in hydrocarbon systems

The pressure decay method has been used to experimentally study molecular diffusion of gases in liquids since it was put forward by Mohammad Riaza in 1996. The experimental setup is simple: a rigid container of constant volume is filled with a certain amount of a specific liquid, and the remaining volume is filled with a specific gas up to a chosen pressure. Temperature is maintained constant throughout the experiment.

Pure diffusion models have been shown to adequately predict results of pressure decay experiments on several hydrocarbon systems [1, 25, 26, 24, 12]. The low molecular weight of the gases compared to the liquids in these systems, in addition the the high liquid viscosity means that advection will be insignificant. Examples of such systems are *gas-oil* and *gas-bitumen* systems. Results gained from such experiments can provide insight into important processes that occur in storage and refining of oil, as well as enhanced oil recovery processes. Since the validity of the assumption that diffusion is the governing transport mechanism has been established in these systems, the models from the previous chapter will first be compared to experimental data for hydrocarbon systems.

4.2 CO_2-bitumen system

As conventional oil reserves decline, bitumen is becoming increasingly important as a source of hydrocarbons. Dissolution of CO_2 in the bitumen reduces the viscosity and can potentially improve recovery. Reliable measurements of diffusivity in bitumen is therefore important for studying processes related to this. Upreti et al., Sheikha et al. and Ghaderi et al. [25, 26, 27] have all focused on CO_2-bitumen systems in their efforts to model pressure decay. The increase in liquid density when CO_2 dissolves in bitumen appears to be negligible based on experimental data by Svrsec et al. [28]. In addition, the viscosity of bitumen is approximately 3 orders of magnitude higher than the viscosity of water. Based on these facts it is reasonable to assume that the forces causing advection will be less dominant in a pressure decay experiment involving CO_2 and bitumen, compared to in a CO_2-water system. Upreti et al. [25] has performed pressure decay experiments on a CO_2-bitumen system under various temperatures. The model put forward in equation (3.14), where interface film resistance has been ignored, has been compared to these experiments. The results can be seen in Figure 13. The Henry's law constant has been estimated based on late time data, and falls within the range of the solubility data reported by Upreti et al. [25]. Compressibility factors in the pressure interval of the experiments are found in [6]. Diffusion coefficients that give the best fit to the experimental data have been chosen. The estimated diffusivities, which are listed in Table 1, are close to those reported by Upreti et al. [29], who reported diffusion coefficients of $1.3 \cdot 10^{-10}\ \frac{\mathrm{m}^2}{\mathrm{s}}$ and $2.3 \cdot 10^{-10}\ \frac{\mathrm{m}^2}{\mathrm{s}}$ at 25°C and 50°C respectively. The match between the model and experimental data is good, which strongly indicates that

the dissolution of CO_2 in bitumen is governed mainly by diffusion. The conditions of the experiment, along with estimated parameters, can be seen in Table 1.

Table 1: Parameters used in the modelling of the pressure decay.

Experimental conditions	25 °C	50 °C
Initial pressure (P_i)	4.12 MPa	3.95 MPa
Gas height (h_G)	0.02 m	0.02 m
Liquid height (h_L)	0.01 m	0.01 m

Estimated parameters	25 °C	50 °C
Henry's law constant (H)	3600 $\frac{m^3Pa}{mol}$	3700 $\frac{m^3Pa}{mol}$
Gas compressibility (Z)	0.80	0.83
Diffusivity (D)	$1.4 \cdot 10^{-10}$ $\frac{m^2}{s}$	$2.6 \cdot 10^{-10}$ $\frac{m^2}{s}$

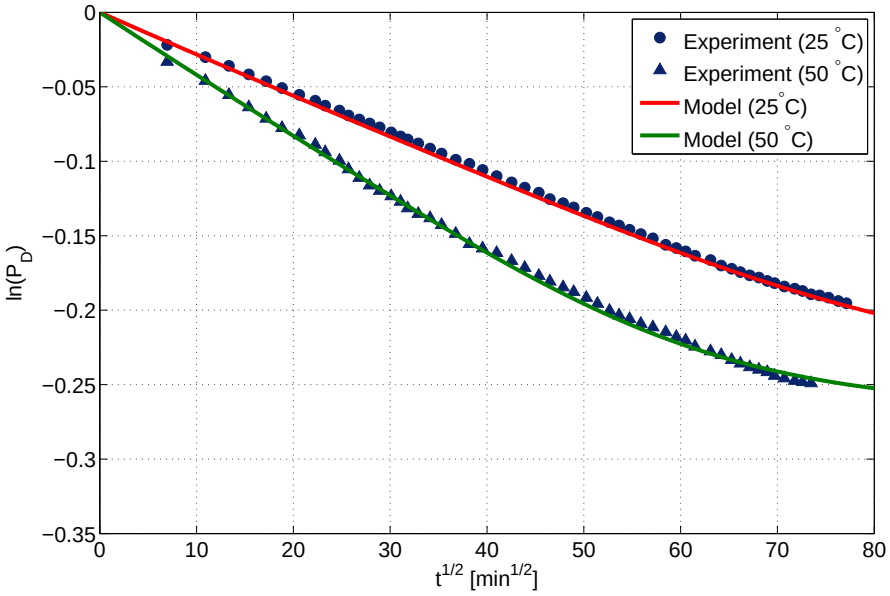

Figure 13: Comparison of model and experimental results in a CO_2-bitumen system. Equation (3.14) is used to model the pressure decay.

4.3 Methane-pentane system

The methane-pentane system was the first to be studied by the method of pressure decay [1]. Advection can be neglected in this system because the liquid density decreases when methane dissolves in pentane. The experimental data from Riazi has been compared to the finite-acting model from Section 3.3. Results can be seen in Figure 14. Late time data has been used to estimate the Henry's law constant to 2870 $\frac{m^3Pa}{mol}$. The compressibility factor of the gas in the pressure interval of the experiment is found in [6]. The diffusion coefficient has been adjusted to a value of $1.05 \cdot 10^{-8}$ $\frac{m^2}{s}$ to fit the experiments. The diffusivity

obtained by Riazi for the same experiment was $1.51 \cdot 10^{-8} \frac{\mathrm{m}^2}{\mathrm{s}}$ [1]. The conditions of the experiment, along with estimated parameters, can be seen in Table 2.

Table 2: Parameters used in the modelling of the pressure decay.

Experimental conditions		Estimated parameters	
Temperature (T)	37.8 °C	Diffusivity (D)	$1.05 \cdot 10^{-8} \frac{\mathrm{m}^2}{\mathrm{s}}$
Initial pressure (P_i)	10.2 MPa	Henry's law constant (H)	2870 $\frac{\mathrm{m}^3\mathrm{Pa}}{\mathrm{mol}}$
Gas height (h_G)	0.1426 m	Gas Compressibility (Z)	0.9
Liquid height (h_L)	0.0768 m		

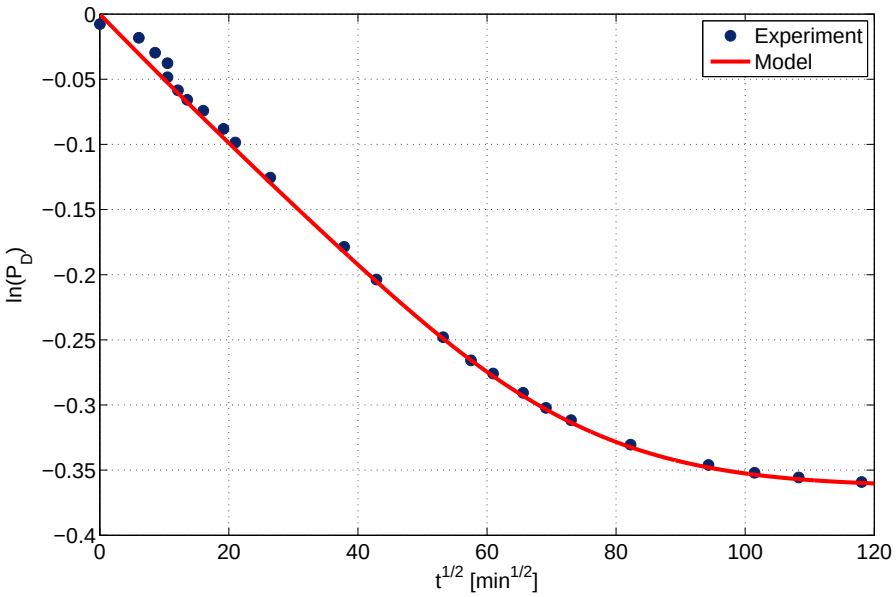

Figure 14: Comparison of experimental and modelling results in a methane-pentane system. Equation (3.14) is used to model the pressure decay.

5 Experimental results (CO_2-water system)

5.1 Pressure decay experiment

Time et al. [4] has performed pressure decay experiments on CO_2-water systems at the University of Stavanger. In the experiments they used a transparent cylinder that was approximately half-filled with distilled water, and CO_2 gas was subsequently injected up to a pressure of approximately 5 bar. A pH indicator was added to the water so that the dissolution could be observed visually (the acidity of the solution will increase with increasing concentration of CO_2). A pressure gauge connected to the cylinder records the pressure drop over time. A photograph of such an experiment can be seen in Figure 15.

As can be seen from Figure 16, the earliest part of the experimental data deviates from the expected straight line behavior. It is unknown whether this can be attributed to an actual physical phenomena, or if it is an effect of the experimental setup. This part of the data has been ignored, except when the experiment is compared to the model with interface film resistance. After a duration of approximately 2 days, the slope of the pressure curve suddenly increases, something which suggests an equipment error, or a sudden change of experimental conditions. This part of the data will be ignored throughout the chapter.

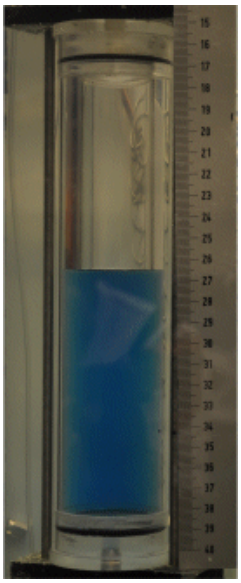

Figure 15: A photograph of the the pressure decay experiment carried out by Time et al.

5.2 Comparing model and experiments

5.2.1 Constant diffusion coefficient

When comparing the results from the mathematical model to the experimental results obtained by Time et al. it is evident that the pressure decay happens

much faster than predicted (see Figure 16). There are two possible explanations for this which are easily recognizable. Since all other parameters are known with a high degree of certainty, the assumed value for the diffusion coefficient may be incorrect. However, values for the diffusion coefficient of carbon dioxide in water that have been reported in the literature [30, 31] are of the same order of magnitude as the one used in the model. In order to get a result that is close to the experiments, a diffusion coefficient that is two orders of magnitude larger must be used. Another explanation is that there are transport phenomena other than pure diffusion that are enhancing the mass transfer of CO_2 into the water. Previous studies have shown that advection currents due to the increased density of water containing CO_2 may play an important role [32]. Figure 16 shows how the model compares with experiments done by Time et al. When standard diffusivity is used, the pressure is at all times predicted to be higher than what the experiments show. When a much higher diffusivity of $2.3 \cdot 10^{-7} \frac{\mathrm{m}^2}{\mathrm{s}}$ is used, the model fits well with the experiments at early times. After about 400 min the slope of the experimental pressure decay decreases, and the model over-predicts the pressure drop. This indicates that advection becomes less dominant as the experiment progresses. It appears from the figure that diffusion alone or a mix of diffusion and advection drives the mass transfer after a certain point. An overview of the physical parameters associated with the experiment can be seen in Table 3.

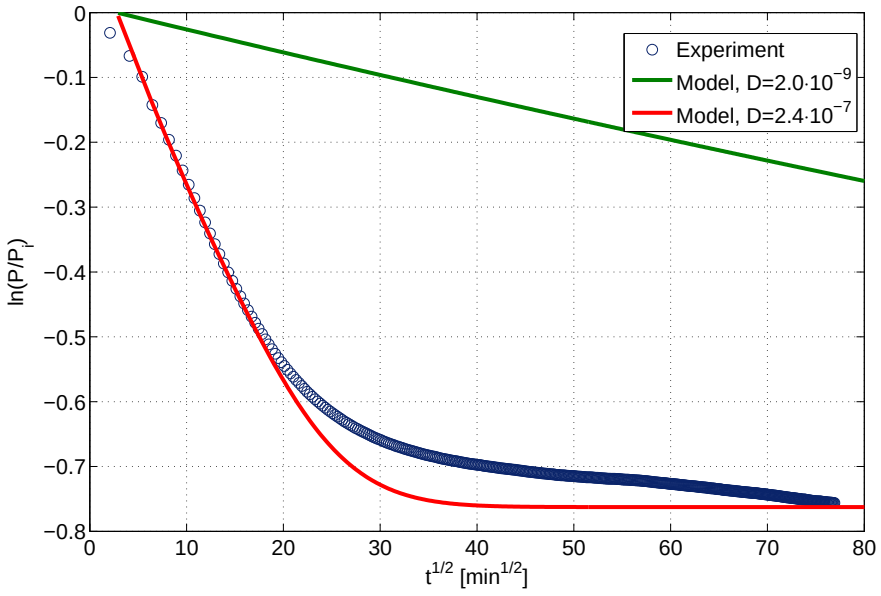

Figure 16: Model compared to experimental data by Time et al. Equation (3.14) is used to model the pressure decay.

5.2.2 Time-dependent diffusion coefficient

A model with time-dependent diffusion coefficient can be utilized in order to gain insight into which transport processes are at work during different time

Table 3: Conditions of pressure decay experiment performed by Time et al.

Experimental conditions		Estimated parameters	
Temperature (T)	21 °C	Henry's constant (H)	2630 $\frac{\mathrm{m^3Pa}}{\mathrm{mol}}$
Initial pressure (P_i)	4.96 bar	Gas Compressibility* (Z)	0.97
Gas height (h_G)	0.097 m	Effective diffusivity** (D)	$2.4 \cdot 10^{-7} \frac{\mathrm{m^2}}{\mathrm{s}}$
Liquid height (h_L)	0.123 m		
Diameter of container	0.05 m		

*Z-factor in pressure interval of experiment is found by interpolation of tables in [6].
**The effective diffusivity that best matches the experimental data at early times.

periods of the experiment. The time-dependent effective diffusivity is assumed to be of the form in equation (5.1). The diffusion coefficient is initially at D_i and goes towards D_f as time increases. Section 3.5 describes how a solution with time-dependent diffusivity is obtained.

$$D(t) = \frac{(D_\mathrm{i} - D_\mathrm{f})\, a^2}{t^2 + a^2} + D_\mathrm{f}. \tag{5.1}$$

The variable τ, necessary to obtain the solution, is calculated as shown below:

$$\tau(t) = \int_0^t D(t')dt' = (D_i - D_f)\, a \arctan\left(\frac{t}{a}\right) + D_\mathrm{f}\, t.$$

The initial diffusion coefficient is set to $2.3 \cdot 10^{-7}\ \frac{\mathrm{m^2}}{\mathrm{s}}$ and the final diffusion coefficient is set to the standard diffusion coefficient for CO_2 in water. The parameter a has units [s], and is adjusted to get the best fit with the experiments. Its value characterizes how long advection will be the dominant transport mechanism. When $t = a$ the difference between the maximum effective diffusivity and the standard molecular diffusivity is halved. For $t \gg a$ the effects of advection will be negligible. For the experiment, the value $a = 2.8 \cdot 10^4$ s was found by visual inspection to give the best fit.

The effective diffusivity from equation (5.1) is shown in Figure 18 as a function of time. This should be an approximation of what the effective diffusivity is during the course of the experiment. The value of the diffusion coefficient gets close to the theoretical value for CO_2 in water towards the end of the experiment, with a final value of $3.3 \cdot 10^{-9}\ \frac{\mathrm{m^2}}{\mathrm{s}}$.

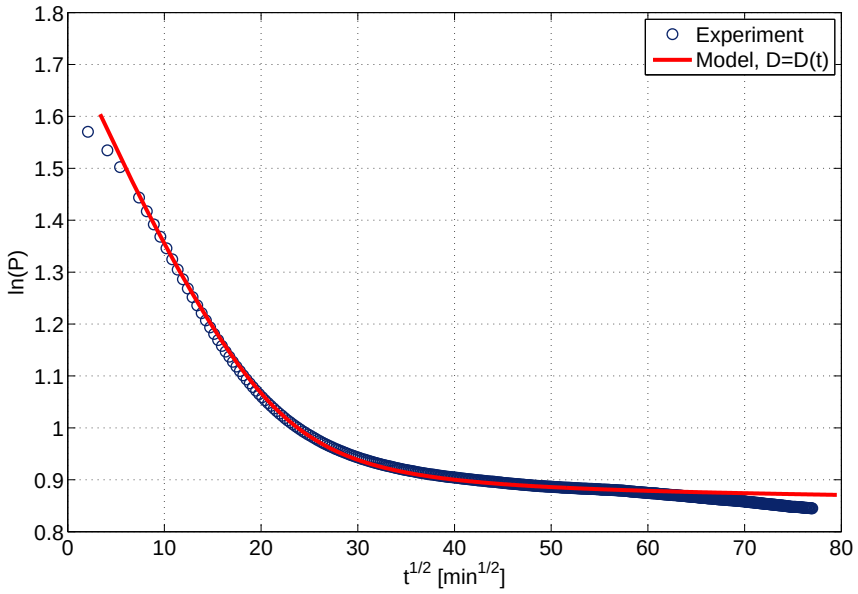

Figure 17: Model with time-dependent diffusion coefficient compared to experimental results. Equation (3.26) is used to model the pressure decay. The effective diffusivity is of the form in equation (5.1), and parameters for the time-dependency of the diffusivity are: $D_\mathrm{i} = 2.3 \cdot 10^{-7}\ \frac{\mathrm{m}^2}{\mathrm{s}}$, $D_\mathrm{f} = 2 \cdot 10^{-9}\ \frac{\mathrm{m}^2}{\mathrm{s}}$, $a = 2.8 \cdot 10^4$ s.

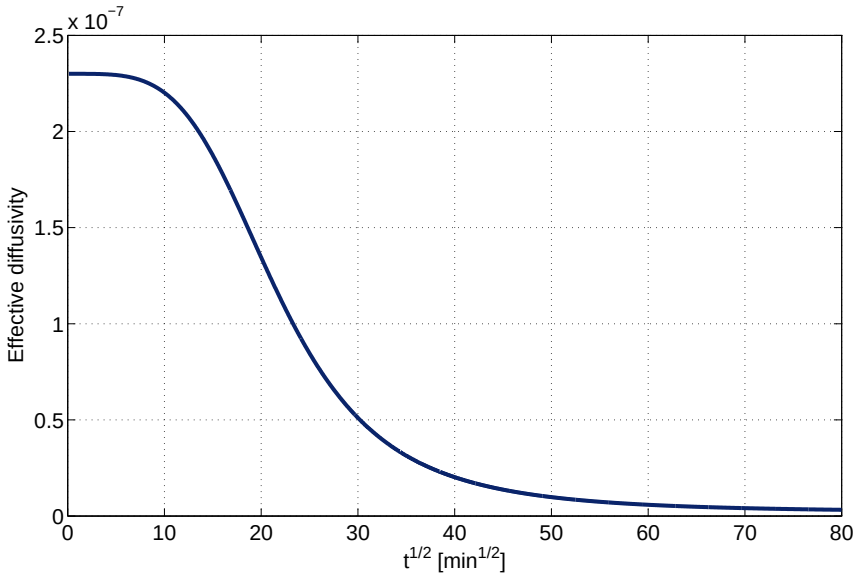

Figure 18: Estimated effective diffusivity over the course of the experiment. The diffusivity becomes $3.3 \cdot 10^{-9}\ \frac{\mathrm{m}^2}{\mathrm{s}}$ towards the end of the experiment.

5.2.3 Late-time transport mechanism

Late-time homogeneous concentration distribution:

In order to investigate which transport mechanisms are at work in the late times of the experiment, the model with initial homogeneous concentration from Section 3.4.1 is applied. If we assume that advection becomes negligible at a certain point, and that the concentration of CO_2 is homogeneously distributed at that point, we can predict how the pressure will evolve from that point forward. The red curve in Figure 19 shows how the pressure would decay if diffusion was the only contributing factor to mass transport. From the figure it seems that the pressure decay resulting from pure diffusion is too low, and that advection still plays a part even in the late times of the experiment. It's unclear whether there is a point in time in which advection becomes negligible compared to diffusion. Another explanation of the fact that pressure declines too rapidly is that the assumption of homogeneous concentration is invalid. If the concentration of CO_2 increases downwards in the container, the the pressure decay, as shown in Figure 19, will be under-predicted and diffusion may still be the dominant transport mechanism.

Late-time heterogeneous concentration distribution:

The model from section 3.4.2 is used to further investigate which transport mechanisms are governing the pressure decay at late times of the experiment. It is plausible that the heavier CO_2-rich water will sink and thus create a scenario where there is a positive concentration gradient towards the bottom of the container at the the point in time in which diffusion becomes the dominant transport mechanism. By looking at different linear concentration profiles and comparing the resulting pressure decay to the experimental data, a possible scenario for late-time diffusion-governed pressure decay has been found. The earliest time at which such a model fit the data was after a run of about 1.5 days, at which point the pressure had decreased from 4.96 bar to 2.44 bar. The result is shown in figure 20. The assumed concentration distribution at the start of the simulation was a concentration of 60.3 $\frac{\text{mol}}{\text{m}^3}$ and a gradient of 381 $\frac{\text{mol}}{\text{m}^4}$ towards the bottom of the container. These values were found by visual inspection to give the best fit with the experimental data. The values corresponds to the total number of moles of CO_2 dissolved in the water as the pressure decreases from 4.96 bar to 2.44 bar. It should be mentioned that the concentration at the bottom of the container in this scenario will be higher than the equilibrium concentration at 2.44 bar. However, a scenario where the CO_2 that was dissolved at an earlier and higher pressure subsequently sunk towards the bottom can justify this concentration.

To determine the initial concentration that is to be used as input to the model, the following expression (which is derived from material balance and the modified ideal gas law) is used:

$$C_{\text{avg}} = \frac{h_{\text{G}}}{h_{\text{L}}} \frac{(P_{\text{i}} - P(t))}{ZRT}.$$

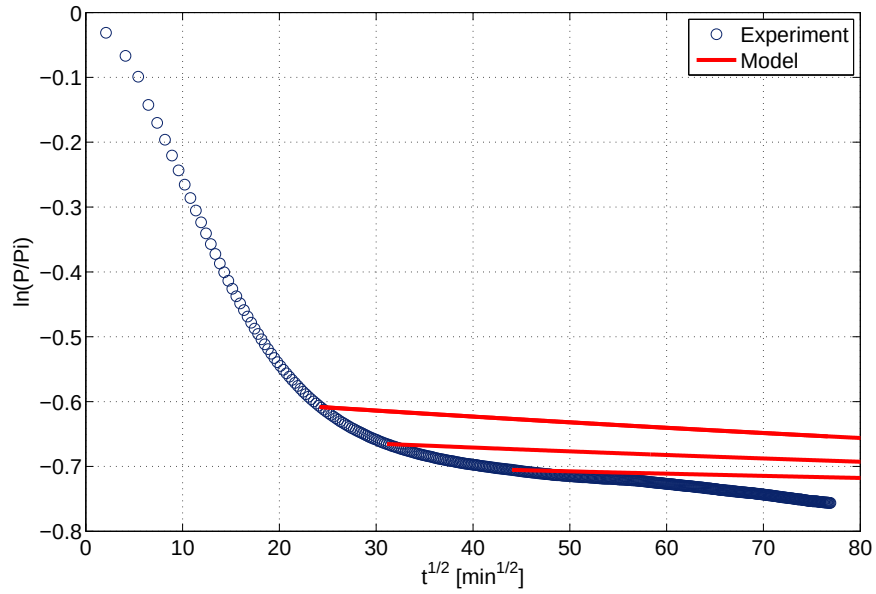

Figure 19: Model with initial homogeneous concentration distribution compared to late-time experiments. Equation (3.17) has been used to model the pressure decay. The predicted pressure decay is too slow, even towards the end of the experiment.

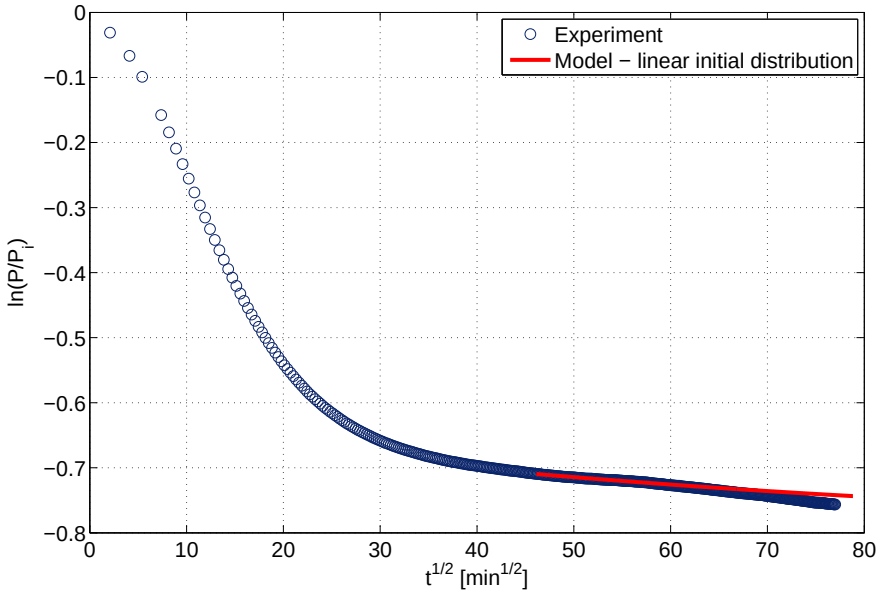

Figure 20: Model with initial linear concentration distribution compared to late-time experiments. Equation (3.21) has been used to model the pressure decay. The concentration distribution parameters at start of simulation is $\kappa_1 = 381\ \frac{\text{mol}}{\text{m}^4}$ and $\kappa_2 = 60.3\ \frac{\text{mol}}{\text{m}^3}$. It can be observed that the model fits well with the experimental data, making it plausible that diffusion is the dominant transport mechanism towards the end of the experiment. The experimental data have been analyzed after $t = 1.3 \cdot 10^5$ s $\gg$ a.

5.2.4 Interface film resistance

The presence of interface film resistance is uncertain. The diffusion model with interface film resistance is compared to the experimental results gathered by Time et al. Results are shown in Figure 21. It is observed from the figure that the early part of the experimental data fits well with the model when interface film resistance is included. This indicates that interface film resistance may be the cause of the gentler slope in the pressure plot at the beginning of the experiment, and thus have a significant impact on the rate of pressure decay in a CO_2-water system. However this result is not conclusive, since it is known that the pressure decay can not be described by diffusion alone. It is also possible that the gentler slope is a result of the experimental setup. Further work should be done in order to investigate the impact of interface film resistance on the CO_2-water system

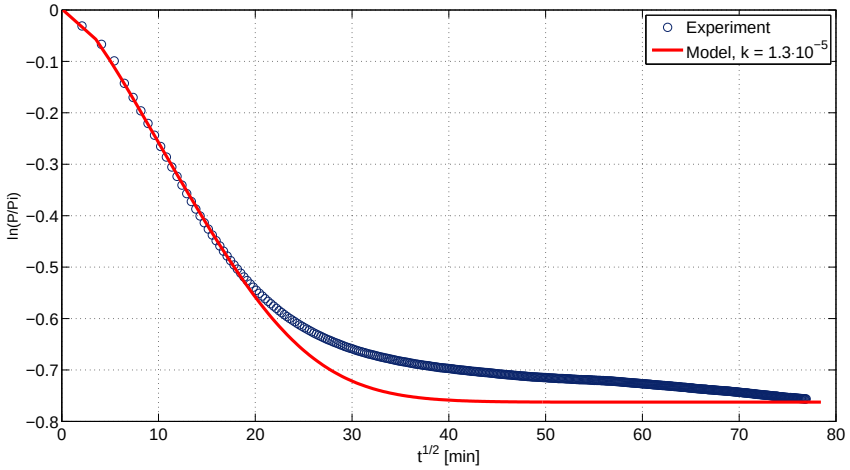

Figure 21: Experimental results compared to the model that includes interface film resistance. Equation (3.36) has been used in the modelling of the pressure decay.

5.3 Obtaining parameters from experimental data

5.3.1 Determination of diffusivity from infinite-acting data

The infinite-acting model from Section 3.2 is dependent on only one relationship: $\frac{ZRT\sqrt{D}}{h_G H}\left(=\frac{1}{\alpha\sqrt{D}}\right)$. All these parameters are known from the experimental setup, except D and H. By analyzing experimental data it is thus possible to estimate a value for the ratio $\frac{\sqrt{D}}{H}$. The infinite acting solution will be valid at early times only, until the diffusing substance reaches the bottom of the container. At early times the solution can be approximated to:

$$\frac{P(t)}{P_i} = \operatorname{erfc}\left(\frac{\sqrt{t}}{\alpha\sqrt{D}}\right). \tag{5.2}$$

when taking use of the fact that

$$\lim_{t\to 0} \exp\left(\frac{t}{\alpha^2 D}\right) = 1.$$

This simplification has been utilized by Sheikha et al. [26] in order to create the following method to graphically determine the diffusion coefficient of gases in bitumen. Taking the inverse complimentary error function of equation (5.2) leads to the expression below:

$$\text{erfc}^{-1}\left(\frac{P(t)}{P_\text{i}}\right) = \frac{\sqrt{t}}{\alpha\sqrt{D}} = \frac{ZRT\sqrt{D}}{h_\text{G}H}\cdot\sqrt{t}.$$

The slope of the straight line in a plot of $\text{erfc}^{-1}\left(\frac{P(t)}{P_\text{i}}\right)$ vs. $\sqrt{t}$ will be $\frac{ZRT\sqrt{D}}{h_\text{G}H}$. The slope, b_1, can be determined graphically and we have

$$\frac{H}{\sqrt{D}} = \frac{ZRT}{b_1 h_\text{G}}.$$

Henry's constant H can be determined from the equilibrium pressure of the system in question, or from tabulated values that exist in the literature. One advantage of this graphical method is that the infinite acting period always produces a straight line, and the infinite acting period ends when the data starts to deviate from this, thus it will always be apparent from the graphical representation in which time intervals this method is applicable. An analogy can be drawn between the method described in this section, and the graphical methods used in the field of well testing.

When applying this method to the experimental results of Time et al., the effective diffusion coefficient at the early part of the experiment can be found. Graphically, the slope has been found to be $3.29\cdot 10^{-3}/\sqrt{s}$ (see Figure 22). The resulting effective diffusion coefficient is determined to be $D = 1.25\cdot 10^{-7}$. This value for the diffusivity is of the same order of magnitude as the one used to fit the model to the data in Section 5.2.1. However, it is still significantly lower, something that suggests that this method should only be used as a quick estimation of diffusivity, and not for detailed analysis.

5.3.2 Determining diffusivity from late-time data

Determination of diffusivity from late time data can prove more difficult than from early data, in that the assumption of infinite liquid height is no longer valid. However, in the case of a CO_2-water system, this is the most interesting period with regards to determining diffusivity. This is due to the fact that advection is potentially less dominant in this time period of the experiment. If the assumption is made that diffusion dominates as the transport mechanism after a certain point, and that the concentration of CO_2 at that point is distributed homogeneously, the diffusion coefficient can be calculated by a modification of the method in the previous section. Since the diffusion process is assumed to begin at the point in question, there will be no error in assuming $h_\text{L}\to\infty$. From equation (3.16) we have that

$$\frac{P(t)-HC_\text{i}}{P_\text{i}-HC_\text{i}} = \exp\left(\frac{t}{\alpha^2 D}\right)\text{erfc}\left(\frac{\sqrt{t}}{\alpha\sqrt{D}}\right) \approx \text{erfc}\left(\frac{\sqrt{t}}{\alpha\sqrt{D}}\right)$$

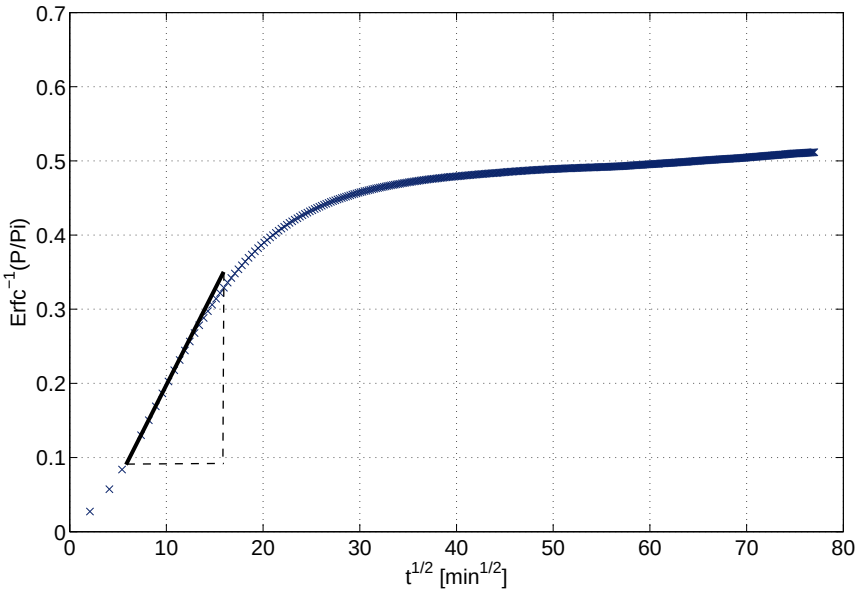

Figure 22: The slope of the straight line in the early parts of the data is calculated in order to estimate the effective diffusivity.

$$\Rightarrow \text{erfc}^{-1}\left(\frac{P(t)-HC_\text{i}}{P_\text{i}-HC_\text{i}}\right) = \frac{ZRT\sqrt{D}}{h_G H}\cdot\sqrt{t}.$$

The slope of $\text{erfc}^{-1}\left(\frac{P(t)-HC_\text{i}}{P_\text{i}-HC_\text{i}}\right)$ vs. $\sqrt{t}$ will then be

$$b_2 = \frac{ZRT\sqrt{D}}{h_G H},$$

and we have

$$D = \left(\frac{b_2 h_G H}{ZRT}\right)^2.$$

Towards the end of the experiment (after 42.25 hours), the pressure has decreased from 4.96 to 2.425 bar. From equation (3.38) we have that the average concentration in the solution is $C_i = 84.4\ \frac{\text{mol}}{\text{m}^3}$. Graphically, the slope is determined to be $b_2 = 5.17\cdot 10^{-4}/\sqrt{\text{s}}$ which leads to a diffusivity of $D = 3.1\cdot 10^{-9}\ \frac{\text{m}^2}{\text{s}}$. This diffusivity is a little higher than the standard reported literature value for CO_2 in water. This is to be expected when considering the results in Section 5.2.3 that indicate that diffusion alone can not be responsible for the mass transfer when there is a homogeneous concentration distribution.

6 Numerical calculations

6.1 Numerical model

Numerical modelling provides the possibility to incorporate additional physical effects that have been difficult to work with analytically. The lattice Boltzmann method has been used in the numerical simulations in this chapter. Matlab code for lattice Boltzmann modelling of the CO_2-water system have been obtained from [33]. When comparing the numerical model with the semi-analytical model from Section 3.3, it can be observed that the results match almost perfectly. In the comparison, the process was modelled numerically as a pure diffusion process, no gravity effects were included, and the same boundary conditions were used as in the semi-analytical model. This result provides a validation of the numerical Lattice Boltzmann model that has been used.

6.2 Lattice Boltzmann modelling

The Lattice Boltzmann method is used for numerical simulation of physical phenomena, primarily in fluid dynamics. The Lattice Boltzmann equation is based on the Lattice Gas Cellular Automata methods[8], and is a relatively recent development. Its use took off in the early 90s. The Lattice Boltzmann equation has in short time evolved into a self-standing research subject in the field of statistical mechanics [34]. Instead of solving the Navier-Stokes equations, like in traditional fluid simulation, fluid flow is simulated using the Boltzmann transport equation[9]. The fluid is modelled using a limited number of fictitious particles confined to a lattice[10]. The particles are represented by a particle velocity distribution function for each component at each grid point. The algorithm for the lattice Boltzmann equation has a 'stream-and-collide' structure. In the first step, particles jump, or stream, to adjacent lattice sites according to the momentum distribution. In the next step, the collision step, momentum distributions are updated. The outcome of collisions are approximated by assuming that momentum of the particles will be redistributed at a constant rate towards an equilibrium distribution f_i^{eq}. The lattice Boltzmann equation can be written as follows [35]:

$$f_{\mathrm{i}}(\vec{x} + \vec{e}\delta_t, t + \delta_t) = f_i(\vec{x}, t) + \frac{1}{\tau_f}(f_{\mathrm{i}}^{\mathrm{eq}} - f_{\mathrm{i}}).$$

The parameter τ_f is called the relaxation time and determines how quickly the momentum distribution approaches equilibrium after each collision. The relaxation time is related to the diffusion coefficient in the following way [36]:

$$\tau_{f,D} = 3D\frac{\delta_t}{\delta_x^2} + \frac{1}{2}.$$

[8] A series of simulation methods consisting of a regular grid of cells which may be in one of a finite number of states (such as 'on' or 'off'). The interest in these methods leveled off when interest the Lattice Boltzmann method started to rise.

[9] The Boltzmann transport equation describes the statistical distribution of one particle in a fluid. The distribution determines the probability of a particle to be at a certain place with a certain velocity.

[10] A lattice model is defined on points on a grid, as opposed to continuous space and time.

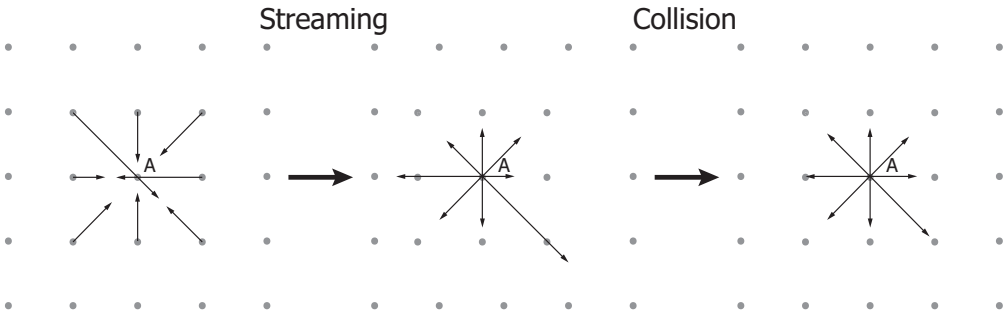

Figure 23: Illustrations of streaming and collision step in lattice Boltzmann model. In the streaming step particles (momenta) are moving into point A. In the collision step the momenta in point A are updated to approach equilibrium.

The space between lattices is denoted δ_x, and the length of the time-steps is denoted δ_t. The Lattice Boltzmann method uses a discrete grid, or lattice as shown in Figure 23. Streaming/collision steps have been illustrated in the figure. Lattice Boltzmann models are commonly classified using a so called DnQm scheme, where n is the number of spacial dimensions and m is the number of directions, or speeds, a particle can travel in. The model in Figure 23 is a D2Q9 model (each node can deliver particles to 8 neighbor nodes in addition to itself). Lattice Boltzmann modelling can be used in most fluid problems, but the method has limitations. In many cases, such as when fluids are highly compressible or there are substantial heat transfer effects, other methods will be more efficient [34]. The Lattice Boltzmann method has proved to be particularly useful when modelling flow in irregular geometries, such as in porous media. Major oil companies have expressed considerable interest in the lattice Boltzmann method as a tool to solve problems related to oil recovery [35].

6.3 Examining solubility simplification

The effects of the simplification done with regards to the solubility of CO_2 in water will be investigated by numerical simulation. The assumption so far has been that the concentrations of HCO_3^- and $CO_3^{2-}$are negligible and will have no significant effect on the rate of pressure decay. Lattice Boltzmann simulations have been run in Matlab, both including and excluding these species. The effect of including these species can be seen in Figure 24. It is apparent that the difference is small, and the error in the value for pressure is well below 0.1 % for the case used in the calculations. Based on this, it can be concluded that the simplifying assumption made in section 2.1 is valid.

6.4 Modelling advection

Several challenges arise when advection is to be included in a lattice Boltzmann model of the CO_2-system in question. In order to achieve numerical stability there are limits to the range of values that can be chosen for the physical parameters. The current version of the numerical lattice Boltzmann model used in this work can not use the physical parameters of the pressure decay experiment

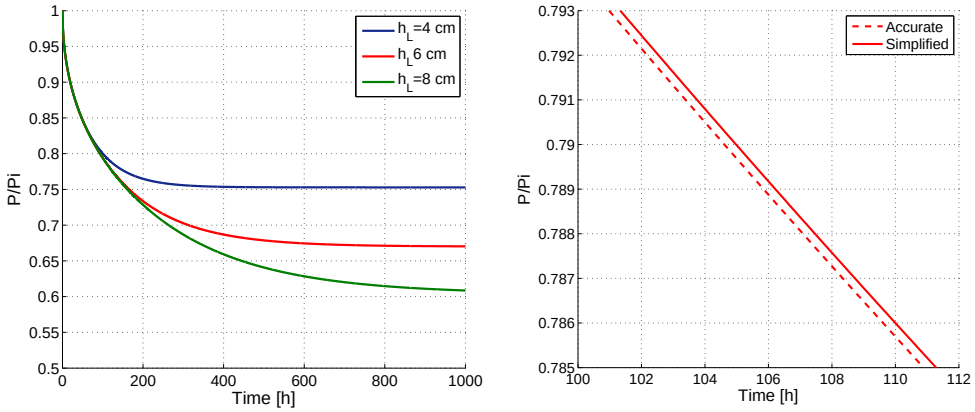

Figure 24: Plots generated with Lattice Boltzmann model (D2Q9). The plot on the right shows discrepancies between the simplified equilibrium calculation used in the analytical model, and a more accurate one. A gas height of 10 cm and a temperature of 25 °C has been used in the calculations. Standard value for diffusivity of CO_2 in water has been used.

without becoming unstable. A plot of the pressure decay in a CO_2-water system when unphysical values are used have been included in Appendix D.

The relaxation time pertaining to the viscosity of the fluid is written in equation (6.1) :

$$\tau_{f,\nu} = 3\nu\frac{\delta_t}{\delta_x^2} + \frac{1}{2}. \tag{6.1}$$

7 Conclusions

An analytical solution to the diffusion equation has been obtained in an effort to model pressure decay in a closed CO_2-water system. Different boundary conditions that include various physical effects and simplifications have been investigated. For the case of finite liquid height a semi-analytical approach was required to obtain the solution. Experimental data has been interpreted qualitatively and quantitatively by making use of the analytical solutions. Numerical modelling of the system in question has also been explored. However, maintaining numerical stability has been problematic when gravitational effects were included.

The mass transfer processes that lead to the pressure decay happens much faster than the analytical model predicts. It can thus be concluded that the pressure decay can not exclusively be described by diffusion. It is believed that advection currents, created by the increased density of water containing CO_2, are causing the enhanced mass transfer. This conclusion is supported by other studies. Although the model has not adequately predicted the pressure decay in a CO_2-water system, it has been useful in illuminating the transport mechanisms at work.

At early times it is clear that advection dominates over diffusion as the main transport mechanism. The dominating transport mechanism at late times is less obvious. As the experiment progresses, and the the solution becomes increasingly saturated with CO_2, the impact of advection appears to decrease . It has been discovered that the pressure decay at late times can not be described by a pure diffusion process if the concentration distribution is assumed to be homogeneous or upwards increasing at that stage of the experiment. However, if the advection currents cause the late-time concentration gradient to be positive in the downward direction, there is still a possibility that advection has ceased towards the end of the experiment, and the pressure decay is at that stage governed by diffusion.

A time-dependent effective diffusion coefficient has been estimated over the course of the experiment. It is found that the effective diffusion coefficient initially is two orders of magnitude larger than the diffusivity of CO_2 in water. The estimated effective diffusivity stays at this value for a certain amount of time before decreasing, ending up at a value close to the literature value towards the end of the experiment. The parameter a, of the model, characterizes the time scale for which advection is dominant. For times $t \gg a$ advection will be negligible.

It has been found that the presence of interface film resistance may explain the unexpected pressure decline rate at the beginning of the experiment. This could, however, also be explained by a late onset of advection, or a weakness in the experimental setup. Further work should be done to investigate if the interface film resistance is significant.

A diffusion-only model is found to give a satisfactory description of pressure decay in a CO_2-bitumen, and a methane-pentane system. The solution found in this work is different from the one originally used to model the methane-pentane system, but predicted values give an excellent match to experimental

results. The essential difference between these experiments and the CO_2-water case, is the significant increase in density that occurs when CO_2 dissolves in water. Such an increase is not present in the other systems, and advection is thus negligible.

Nomenclature

α Group of coefficients

β Expansion coefficient

δ_t Time step

δ_x Lattice spacing

κ_1 Concentration gradient [mol/m^4]

κ_2 Surface concentration [mol/m^3]

ν Kinematic viscosity

ρ Density [kg/m^3]

τ Transformed time variable [m^2]

τ_f Relaxation time

A Area of interface [m^2]

a Chemical activity

A^* Rate of concentration change [mol/s]

b Slope

C Concentration [mol/m^2]

D Diffusivity [(m^2/s)]

f Particle distribution function

H Henry's law constant [Pa $\cdot$ m^3/mol]

h_{G} Gas height [m]

h_{L} Liquid height [m]

J Molar flux [mol/(m$^2\cdot$s)]

K Chemical equilibirium constant

k Mass transfer coefficient [m/s]

m Molarity [mol/m^3]

n Number of moles [mol]

P Partial pressure [Pa]

p Partial pressure [atm]

S Surface [m^2]

s Laplace frequency variable [1/s]

T Temperature [K]

t Time [s]

V Volume [m^3]

Z Gas compressibility factor

Re Rayleigh number

References

[1] M. R. Riazi. A new method for experimental measurement of diffusion coefficients in reservoir fluids. *Journal of Petroleum Science and Engineering*, 14(3-4):235 – 250, 1996.

[2] S. Reza Etminan, Brij B. Maini, Zhangxin Chen, and Hassan Hassanzadeh. Constant-pressure technique for gas diffusivity and solubility measurements in heavy oil and bitumen. *Energy & Fuels*, 24:533–549, 2010.

[3] R. Farajzadeh, A. Barati, H. A. Delil, Bruining, J., and Zitha. Mass transfer of CO_2 into water and surfactant solutions. *Petroleum Science and Technology*, 25(12):1493–1511, 2007.

[4] R. Time and A. H. Rabenjafimanantsoa. Paper in preparation. University of Stavanger.

[5] R. M. Garrels and C. L. Christ. *Solutions Minerals and Equilibria*. Freeman Cooper Co, 1982.

[6] R. H. Perry and D. W. Green. *Perry's Chemical Engineers' Handbook*. McGraw Hill, 1999.

[7] J. Crank. *The Mathematics of Diffusion*. Oxford University Press, 1975.

[8] P. Papatzacos. *Mathematical Modelling*. University of Stavanger, 2008.

[9] F. P. Incropera and D. P. DeWitt. *Fundamentals of heat and mass transfer*. Wiley, 1990.

[10] J. M. Simon, D. Bedeaux, S. Kjelstrup, J. Xu, and E. Johannessen. Interface film resistivities for heat and mass transfersintegral relations verified by non-equilibrium molecular dynamics. *The Journal of Physical Chemistry B*, 110(37):18528–18536, 2006.

[11] S. R. Etminan, M. Pooladi-Darvish, B. Maini, Z. Chen, SPE, and University of Calgary. Mass diffusion parameters in presence of interface resistance in gas-bitumen systems. *Canadian Unconventional Resources & International Petroleum Conference*, 2010.

[12] F. Civan and M. L. Rasmussen. Accurate measurement of gas diffusivity in oil and brine under reservoir conditions. *SPE 67319, SPE Production and Operations Symposium, Oklahoma City, Oklahoma*, 24-27 March 2001.

[13] S. Chandrasekhar. *Hydrodynamic and Hydromagnetic Stability*. Dover Publications, 1981.

[14] A. V. Getling. *Rayleigh-Benard Convection: Structures and Dynamics*. World Scientific, 1998.

[15] M. Abramowitz and I. A. Stegun. *Handbook of Mathematical Functions with Formulas, Graphs, and Mathematical Tables*. Dover Publications, 1964. Electronic copy. http://people.math.sfu.ca/~cbm/aands/ [accessed 02.16.2011].

[16] W. Srigutomo. Gavsteh.m: Gaver-stehfest algorithm for inverse laplace transform (Matlab function), 2006. http://www.mathworks.com/matlabcentral [accessed 02.28.2011].

[17] K. J. Hollenbeck. Invlap.m: A matlab function for numerical inversion of laplace transforms by the de Hoog algorithm, 1998. http://www.isva.dtu.dk/staff/karl/invlap.htm [accessed 02.28.2011].

[18] F. Oberhettinger and L. Badii. *Tables of Laplace Transforms.* Springer-Verlag Berlin Heidelberg New York, 1973.

[19] H. Sheikha, A. K. Mehrotra, and M. Pooladi-Darvish. An inverse solution methodology for estimating the diffusion coefficient of gases in athabasca bitumen from pressure-decay data. *Journal of Petroleum Science and Engineering*, 53(3-4):189 – 202, 2006.

[20] M. L. Rasmussen and F. Civan. Parameters of gas dissolution in liquids obtained by isothermal pressure decay. *AIChE Journal*, 55(1):9–23, 2009.

[21] E. Veling. Analytical solution and numerical evaluation of the radial symmetric convection-diffusion equation with arbitrary initial and boundary data. *Impact of Human Activity on Groundwater Dynamics (Proceedings of Symposium S3 during the 6th Scientific Assembly of the International Association of Hydrological Sciences). IAHS Publ.*, no. 269, 2001.

[22] A. P. Prudnikov, Y. A. Brychkov, and O. I. Marichev. *Integrals and Series: Inverse Laplace Transforms.* CRC, 1992.

[23] A. K. Tharanivasan, C. Yang, and Y. Gu. Comparison of three different interface mass transfer models used in the experimental measurement of solvent diffusivity in heavy oil. *Journal of Petroleum Science and Engineering*, 44(3-4):269 – 282, 2004.

[24] Y. P. Zhang, C. L Hyndman, and B. B. Maini. Measurement of gas diffusivity in heavy oils. *Journal of Petroleum Science and Engineering*, 25(1-2):37 – 47, 2000.

[25] S.R. Upreti and A. K. Mehrotra. Experimental measurement of gas diffusivity in bitumen: Results for carbon dioxide. *Ind. Eng. Chem. Res.*, 39:1080–1087, 2000.

[26] H. Sheikha, M. Pooladi-Darvish, and A. K. Mehrotra. Development of graphical methods for estimating the diffusivity coefficient of gases in bitumen from pressure-decay data. *Energy & Fuels*, 19:2041–2049, 2005.

[27] S. M. Ghaderi, S. H. Tabatabaie, H. Hassanzadeh, and M. Pooladi-Darvish. Estimation of concentration-dependent diffusion coefficient in pressure-decay experiment of heavy oils and bitumen. *Fluid Phase Equilibria*, In Press, Corrected Proof, 2011.

[28] W. Y. Svrcek and A. K. Mehrotra. Gas solubility, viscosity and density measurements for athabasca bitumen. *Journal of Canadian Petroleum Technology*, 1982.

[29] S. R. Upreti and A. K. Mehrotra. Diffusivity of CO_2, CH_4, C_2H_6 and N_2 in athabasca bitumen. *The Canadian Journal of Chemical Engineering*, 80:116–125, 2002.

[30] W. J. Thomas and M. J. Adams. Measurement of the diffusion coefficients of carbon dioxide and nitrous oxide in water and aqueous solutions of glycerol. *Trans. Faraday Soc.*, 61:668–673, 1965.

[31] M. Frank, J. Kuipers, and W. van Swaaij. Diffusion coefficients and viscosities of CO_2 + H_2O, CO_2 + CH_3OH, NH_3 + H_2O, and NH_3 + CH_3OH liquid mixtures. *J. Chem. Eng. Data*, 41:297–302, 1996.

[32] R. Farajzadeh, H.A. Delil, P.L.J. Zitha, and J. Bruining. Enhanced mass transfer of CO_2 into water and oil by natural convection. *EUROPEC/EAGE Conference and Exhibition, London*, SPE 107380, 2007.

[33] Janne Pedersen. Personal communication.

[34] S. Succi. *The lattice Boltzmann equation for fluid dynamics and beyond.* Clarendon Press, 2001.

[35] S. Chen, G. D. Doolen, and K. G. Eggert. Lattice-boltzmann fluid dynamics - a versatile tool for multiphase and other complicated flows. *Los Alamos Science*, 22, 1994.

[36] Dieter Wolf-Gladrow. A lattice boltzmann equation for diffusion. *Journal of Statistical Physics*, 79:1023–1032, 1995.

[37] Y. Song, M. Nishio, B. Chen, S. Someya, and T. Ohsumi. Measurement on CO_2 solution density by optical technology. *Journal of Visualization*, 6:41–51, 2003.

A Rayleigh-Bénard Instability

The onset of the Rayleigh-Bénard instability is determined by a critical value of the dimensionless Rayleigh number . The Rayleigh number of a layer heated from below is defined as [13]:

$$\mathrm{Ra} = \left|\frac{dT}{dx}\right| \cdot \frac{g\beta_\mathrm{t}}{\nu D_\mathrm{t}} h_\mathrm{L}^4,$$

where g is the acceleration due to gravity, β_t is the thermal expansion coefficient, ν is the kinematic viscosity, D_t is the thermal diffusivity, and h_L is the thickness of the layer. The definition of Re is arbitrarily chosen, but proves useful in a number of scenarios. An analogous Rayleigh number, useful when dealing with the CO_2-water system, would thus be:

$$\mathrm{Ra} = \left|\frac{dC}{dx}\right| \cdot \frac{g\beta_\mathrm{c}}{\nu D} h_\mathrm{L}^4, \tag{A.1}$$

with $\beta_\mathrm{c} = \frac{1}{V}\frac{dV}{dC}$ being the concentration expansion coefficient. The critical Rayleigh number for the onset of Rayleigh-Bénard instability in a system with one rigid and one free surface (similar to the CO_2-water system in this study) has been determined to be $\mathrm{Ra}_\mathrm{crit} = 1100.65$ by S. Chandrasekhar [13]. For a system with bounding vertical surfaces, such as a vertical cylinder, the Rayleigh number will effectively be lower than is calculated by equation (A.1), and a larger density gradient is required before advection occurs. However, calculated Rayleigh numbers may still in many cases give a good idea of whether or not advection develops.

A density correlation put forward by Song et al. [37] is used in order to estimate β_c, a parameter needed to calculate the Rayleigh number. Song et al. reported the density of water with dissolved CO_2 relative to that of pure water to be:

$$\frac{\rho}{\rho_0} = 1 + 0.275 X_{\mathrm{CO}_2},$$

where X_{CO_2} is the mass fraction of CO_2 in the solution. The expression below describes the density as a function of concentration $\left(\frac{\mathrm{mol}}{\mathrm{m}^3}\right)$ instead of mass fraction. The density of pure water has, for simplicity, been used when converting from mass fraction to concentration.

$$\begin{aligned} \frac{\rho}{\rho_0} &= 1 + 1.21 \cdot 10^{-5}\ \frac{\mathrm{m}^3}{\mathrm{mol}} \cdot C \\ \Rightarrow\ V(C) &= \frac{V_0}{1 + 1.21 \cdot 10^{-5}\ \frac{\mathrm{m}^3}{\mathrm{mol}} \cdot C} \end{aligned}$$

The concentration expansion coefficient becomes

$$\beta_\mathrm{c} = \frac{1}{V}\frac{dV}{dC} = \frac{1}{\left(\frac{1}{1.21 \cdot 10^{-5}}\ \frac{\mathrm{mol}}{\mathrm{m}^3} + C\right)} \approx 1.21 \cdot 10^{-5}\ \frac{\mathrm{m}^3}{\mathrm{mol}}.$$

An approximation of the Rayleigh number defined in equation (A.1) that is associated with the pressure decay experiment by Time et al. can be given by the following expression:

$$\mathrm{Ra} = (C_{\mathrm{top}} - C_{\mathrm{buttom}}) \cdot \frac{g\beta_{\mathrm{c}}}{\nu D} h_{\mathrm{L}}^3 = \frac{P_{\mathrm{i}}}{H} \cdot \frac{g\beta_{\mathrm{c}}}{\nu D} h_{\mathrm{L}}^3$$

The Rayleigh number for the experiment can now be calculated:

$$\mathrm{Ra} = 1.13 \cdot 10^9 \gg \mathrm{Ra}_{\mathrm{crit}}.$$

Calculations show that the Rayleigh number is much larger than the critical Rayleigh number (6 orders of magnitude larger). Based on this, the assumption can be made that advection currents develop during the course of the experiment.

B Physical properties of CO_2

Solubility

Table 4: Solubility parameters at 2.3 bar.

	$21°C$
$K_{CO_2(g)}$	$10^{-7.87}$
$K_{H_2CO_3}$	$10^{-6.45}$
H	2630 $\frac{m^3Pa}{mol}$

Diffusivity

The diffusion coefficient of CO_2 in water at standard conditions is $D = 2{\cdot}10^{-9}\,\frac{m^2}{s}$ [30] .

Solution density

The correlation between density and mass fraction of CO_2 in an aqueous solution [37]:

$$\frac{\rho}{\rho_0} = 1 + 0.275 X_{CO_2},$$

Compressibility

Table 5: Compressibility factors (Z-factors) for CO_2. Data obtained from [6].

	Pressure [bar]			
Temp. [°C]	1	5	10	20
0	0.9933	0.9658	0.9294	0.8496
50	0.9964	0.9805	0.9607	0.9195
100	0.9977	0.9883	0.9764	0.9524

C Additional modelling

Model with time-dependent diffusivity and interface film resistance

When interface film resistance is added to the model with time-dependent diffusion coefficient, the Laplace transformed solution is as follows. Note that in order to acquire the expression below, the diffusivity at the interface film, D^*, must be considered constant, while the diffusivity in the rest of the water phase is variable. This is a simplification done for mathematical reasons and may have no physical basis. The equations presented here are therefore currently not considered applicable to any physical problem.

The expression for pressure decay is in this case:

$$\overline{P}(s_\tau) = \frac{P_\mathrm{i}\left[(e^{-2\sqrt{S_\tau}h_\mathrm{L}}+1) - \frac{D^*}{k}\left(\sqrt{S_\tau}e^{-2\sqrt{S_\tau}h_\mathrm{L}} - \sqrt{S_\tau}\right)\right]}{s + \left(\frac{1}{\alpha_\tau} + \frac{D*S_\tau}{k}\right)\sqrt{S_\tau} + e^{-2\sqrt{S_\tau}h_\mathrm{L}}\left[S_\tau - \left(\frac{1}{\alpha_\tau} + \frac{D(t)S_\tau}{k}\right)\sqrt{S_\tau}\right]} \quad \text{(C.1)}$$

The boundary condition at the interface is derived using the methods described in Sections 3.5 and 3.6, and is:

$$\frac{\partial \overline{C}}{\partial x}\Big|_{x=0} = \frac{\alpha_\tau}{(1+\frac{\alpha_\tau D^*}{k}s)}(s\overline{C} - \frac{P_\mathrm{i}}{H})\Big|_{x=0}.$$

Figure25 shows results obtained from equation (C.1) compared to experimental results. Equation (5.1) has been used as the time-dependent function for diffusivity, with $a = 4.1 \cdot 10^4$ s (which is higher than the value for a previously used in this work). The diffusivity at the interface is set to $D^* = 2.3 \cdot 10^{-7}\ \frac{\mathrm{m}^2}{\mathrm{s}}$, and all other parameters are the same as used in Section 5.2.2. A good match can be observed between predicted and measured values.

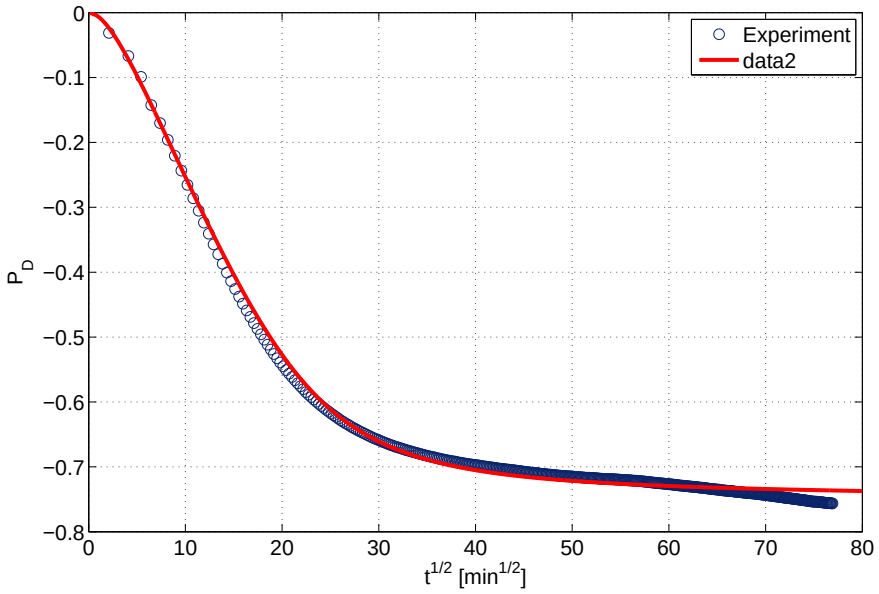

Figure 25: Model with time-dependent diffusivity and interface film resistance compared to experimental results.

D Supplementary plots

Lattice Boltzmann simulation with gravitational effects

Parameters are listed in Table 6. Simulations are done on a box of with sides of $L = 0.4\,\mathrm{m}$.

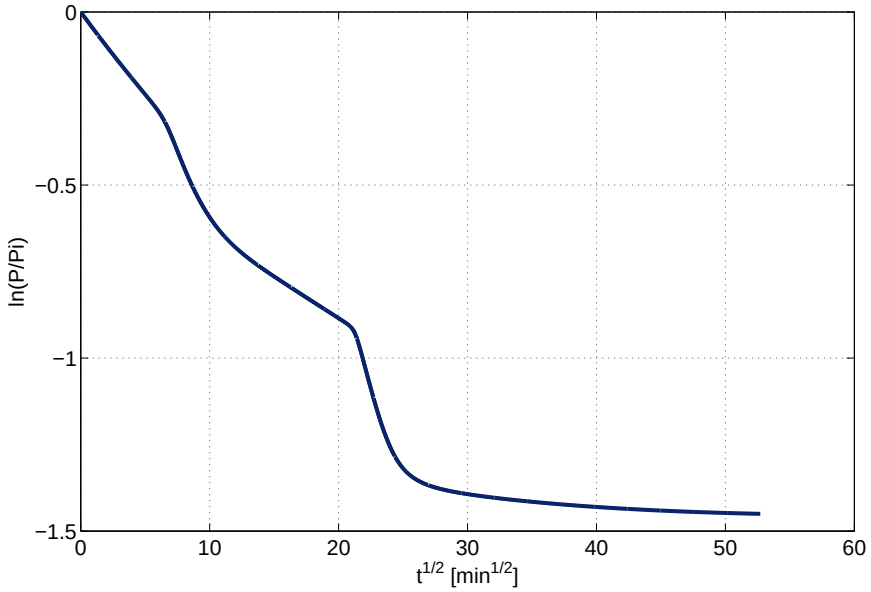

Figure 26: Lattice Boltzmann simulation of pressure decay in a CO_2 system. Advection is included. Matlab code for simulation is obtained from [33].

Table 6: Parameters used in the lattice Boltzmann simulation.

D	$5 \cdot 10^{-7}\ \frac{\mathrm{m}^2}{\mathrm{s}}$	L	$0.4\,\mathrm{m}$
ν	$10^{-6}\ \frac{\mathrm{m}^2}{\mathrm{s}}$	g	$10^{-3}\ \frac{\mathrm{m}}{\mathrm{s}^2}$